The chirality of the mitotic spindle provides a passive mechanical response to forces and depends on microtubule motors and crosslinkers

Monika Trupinić[1], Barbara Kokanović[1], Ivana Ponjavić[1], Ivan Barišić[2], Siniša Šegvić[2], Arian Ivec[3], Iva M. Tolić[1]

[1]Ruđer Bošković Institute, Zagreb, Croatia
[2]Department of Electronics, Microelectronics, Computer and Intelligent Systems, Faculty of Electrical Engineering and Computing, University of Zagreb, Croatia
[3]Department of Physics, Faculty of Science, University of Zagreb, Croatia

ABSTRACT

Mechanical forces produced by motor proteins and microtubule dynamics within the mitotic spindle are crucial for the movement of chromosomes and their segregation into the daughter cells. In addition to linear forces, rotational forces or torques are present in the spindle, reflected in the left-handed twisted shapes of microtubule bundles that make the spindle chiral. However, the biological role and molecular origins of spindle chirality are unknown. By developing methods to measure spindle twist, we show that spindles are most chiral near the metaphase-to-anaphase transition. To test whether spindles react to external forces by changing the twist, we compressed the spindles along their axis, which resulted in stronger left-handed twist. Inhibition or depletion of motor proteins that perform chiral stepping, Eg5/kinesin-5 or Kif18A/kinesin-8, decreased the left-handed twist or led to right-handed twist, suggesting that these motors regulate the twist by rotating microtubules around one another within the antiparallel overlaps. Right-handed twist was also observed after depletion of the microtubule crosslinker PRC1 or the nucleator augmin, indicating that PRC1 contributes to the twist by constraining microtubule rotation, and augmin by nucleating antiparallel bridging microtubules. The observed switch from left-handed to right-handed twist reveals the existence of competing mechanisms that promote twisting in opposite directions. As round spindles were more twisted than elongated ones, we suggest that bending and twisting moments are generated by similar molecular mechanisms. We propose a physiological role for spindle chirality in providing a passive mechanical response to forces, decreasing the risk of spindle breakage under high load.

INTRODUCTION

Mitosis is a stage of the cell cycle in which replicated chromosomes are separated into two new nuclei destined to the two daughter cells (Nurse, 2000). In order to segregate the genetic material, the cell forms a mitotic spindle, a complex micro-structure made of microtubules and numerous associated proteins (McIntosh et al., 2012; Pavin and Tolic, 2016; Prosser and Pelletier, 2017). The spindle physically separates the chromosomes to the opposite poles of the cell and ensures that each daughter cell has the same number of chromosomes as the parental cell.

The spindle is a mechanical structure that can generate and balance forces within itself (Pavin and Tolic, 2021). Forces in the spindle are crucial for proper spindle functioning in each phase of mitosis. Kinetochore fibers exert forces necessary for the positioning of the chromosomes at the center of the spindle in metaphase (Maiato et al., 2017; Risteski et al., 2021) and for pulling the chromosomes apart during anaphase (Asbury, 2017; Vukusic et al., 2019). On the other hand, overlap bundles balance the forces at kinetochores by acting as bridges between sister kinetochore fibers in metaphase and anaphase (Kajtez et al., 2016; Polak et al., 2017; Simunic and Tolic, 2016; Tolic, 2018; Vukusic et al., 2017), and also regulate pole separation in anaphase (Scholey et al., 2016; Vukusic et al., 2021; Vukusic and Tolic, 2021). All the forces in the spindle arise from active processes of motor proteins as well as microtubule polymerization and depolymerization (Howard, 2001; Tolic-Norrelykke, 2008). Direct measurement of the forces in the spindle, although possible (Nicklas, 1983), is challenging because of the small scales involved.

Forces are also responsible for the shape of a spindle. Due to the mechanical properties of microtubules, which are thin and elastic filaments that are inherently straight and curve under forces, the spindle obtains its characteristic shape (Kajtez et al., 2016; Rubinstein et al., 2009). This means that the spindle shape reflects the forces within it, which allows for an indirect measurement of forces by inferring them from the shapes of the microtubule bundles (Kajtez et al., 2016; Tolic et al., 2019), similarly to studies of forces and shapes of individual microtubules *in vitro* (Dogterom and Yurke, 1997; Gittes et al., 1993).

Recently, it was shown that the shape of the mitotic spindle in human HeLa and U2OS cells is chiral, as the spindle has a left-handed twist around the pole-to-pole axis (Novak et al., 2018). Microtubule bundles twist because of the torques that exist within them in addition to linear forces. The experimentally measured three-dimensional shapes of the microtubule bundles, primarily bridging fibers that laterally link sister kinetochore fibers, were used to deduce forces and torques in the spindle by comparison with a theoretical model (Novak et al., 2018). Left-handed twist was also observed in spindles lacking NuMA and kinesin-5 activity in RPE1 cells during metaphase and anaphase (Neahring et al., 2021). Another organism whose spindles are prominently twisted is a unicellular eukaryote, amoeba *Naegleria gruberi*. Interestingly, amoeba's spindles are predominantly twisted in a right-handed fashion (Velle et al., 2021).

The twist of the spindle is potentially generated by motor proteins that, in addition to linear forces, exert rotational forces on microtubules by switching protofilaments with a bias in a certain direction (Bormuth et al., 2012; Brunnbauer et al., 2012; Bugiel et al., 2015; Can et al., 2014; Maruyama et al., 2021; Mitra et al., 2020; Mitra et al., 2018; Ramaiya et al., 2017; Vale and Toyoshima, 1988; Walker et al., 1990; Yajima and Cross, 2005; Yajima et al., 2008). The first molecular motor discovered to generate torque was the single-headed axonemal dynein. In *in vitro* gliding motility assays, surface-attached dynein motors rotated the microtubules around their axis in a clockwise motion, when viewed from the minus-end of the microtubules, while translocating them in a linear fashion (Vale and Toyoshima, 1988). The same type of assay was used to show that the minus-end directed motor kinesin-14 (Ncd) generates torques which rotate microtubules in a clockwise direction as viewed from their minus-ends (Walker et al., 1990), and similar results were obtained with kinesin-14 in an assay in which microtubules glide along each other, where the transport microtubule moves in a helical motion in a clockwise direction (Mitra et al., 2020).

Counterclockwise rotation direction has been found for the plus-end-directed motor protein kinesin-5 (Eg5), which was observed as a corkscrew motion of a sliding microtubule on surface-attached motors (Yajima et al., 2008). Gliding motility assays, as well as motility assays on freely suspended microtubules, showed a counterclockwise rotation for the plus-end-directed motor protein kinesin-8 (Kip3) (Bormuth et al., 2012; Mitra et al., 2018), while another study found that kinesin-8 can switch protofilaments in both directions (Bugiel et al., 2015). Several other motor proteins also exhibit rotational movements, including kinesin-1 (Ramaiya et al., 2017; Yajima and Cross, 2005), kinesin-2 (Brunnbauer et al., 2012), cytoplasmic dynein (Can et al., 2014), and kinesin-6 (MKLP1) (Maruyama et al., 2021). However, in contrast to this large body of knowledge on chiral motor stepping *in vitro*, the role of motor proteins and their asymmetric stepping in the generation of torques within microtubule bundles *in vivo* and consequently spindle twist is unknown.

In this paper we address the molecular origin and the biological role of spindle chirality. We show that spindle twist changes through different phases of mitosis and peaks around anaphase onset in a cancer and a non-cancer cell line. Round spindles were more twisted than elongated ones, which we explored further by compressing the spindle along the pole-to-pole axis, which resulted in a stronger left-handed twist. By performing a candidate screen in which we depleted or inactivated motor proteins that step in a chiral manner and other microtubule-associated proteins involved in the bridging fiber formation, we identified several molecular players involved in the regulation of spindle chirality. Inhibition of Eg5 or depletion of Kif18A decreased the left-handed twist or abolished twist in HeLa cells, respectively, and resulted in zero twist or right-handed twist in RPE1 cells. Thus we propose that these motors regulate twist by rotation of microtubules around one another within the antiparallel overlaps of bridging fibers. Depletion of the main crosslinker of antiparallel microtubules, Protein Regulator of Cytokinesis 1 (PRC1), resulted in right-handed twist in RPE1 cells, indicating that PRC1 may

contribute to the twist by constraining free rotation of microtubules within the bridging fibers. Overexpression of PRC1 abolished twist, which may be due to an increased number of bundled microtubules and thus increased torsional rigidity of the bundles. Depletion of augmin, a protein complex required for the formation of bridging microtubules, abolished the twist of HeLa spindles and led to right-handed twist of RPE1 spindles, suggesting that twist is affected by the reduced number of microtubules in bridging fibers. Finally, we propose a biological function of spindle chirality in promoting the flexibility of the spindle and its passive mechanical response to external forces, thereby decreasing the risk of spindle breakage under high load.

RESULTS

Spindle twist is most pronounced at anaphase onset in cancer and non-cancer cell lines

To explore the twist of the spindle, the first step was to obtain end-on view images covering the whole spindle from pole to pole because this view allows for the visualization of the twist of microtubule bundles (Fig. 1A, end-on view; Movie S1). A signature of the twisted shape is that microtubule bundles look like flower petals in the end-on view. In contrast, the twisted shape is not easily recognized in the side-view of the spindle (Fig. 1A, side view). If the spindle is standing vertically with respect to the imaging plane, a z-stack of images directly provides an end-of view of the spindle, but if the spindle is lying horizontally, a z-stack needs to be transformed into the end-on view.

To quantify spindle twist, we used 3 complementary approaches: visual assessment, optical flow, and bundle tracing (Fig. S1A; Methods). In the visual assessment method, the spindle is observed end-on and the rotation of microtubule bundles around the pole-to-pole axis is estimated visually. If the bundles rotate clockwise when moving along the spindle axis in the direction towards the observer, the twist is left-handed, and vice versa (Fig. S1A, left). We score the twist as strong left-handed, weak left-handed, strong right-handed, weak right-handed, or no visible twist, and use this method as a quick estimate of twist and as a control for other methods. In the optical flow method, the movement of the signal coming from microtubule bundles is estimated by comparing the signal from one z-plane to the next (Fig. S1A, middle; Methods). This method provides a value for the average twist of all bundles in a spindle and is optimal for experiments on a large number of spindles because it is automated. The bundle tracing method is an extension of the approach developed previously (Novak et al., 2018), where individual bundles are manually traced by following the bundle contour in the end-on view of the spindle (Fig. S1A, right; Methods). Subsequently, each bundle is analyzed so that a plane is fitted to the points representing the bundle, and a circle that lies within this plane is fitted to these points and used to calculate the curvature and twist of individual bundles (Ivec et al., 2021) (Fig. S1A, right; Methods).

As a label for microtubule bundles, we used SiR-tubulin to observe all microtubule bundles, or PRC1-GFP to observe the bridging fibers (Kajtez et al., 2016; Polak et al., 2017). To compare the results of the three methods, we analyzed twist of 10 metaphase spindles in HeLa cells stably expressing PRC1-GFP (Fig. S1B). All three methods yielded a left-handed twist, which is expressed by negative values, for all 10 spindles. The spindles that were visually assessed as having a strong left twist had, on average, a higher left twist value also in the bundle tracing and optical flow method, than those with a weak left twist. The absolute values of twist of individual spindles obtained by bundle tracing and optical flow were similar, with optical flow yielding smaller negative values (-1.32 ± 0.29 °/μm, n = 10; all data are given as mean ± sem) than bundle tracing (-2.07 ± 0.29 °/μm, n = 10). This difference is likely due to the sensitivity of the optical flow method to all signal including the background. Based on this cross-check between the three methods, we conclude that they provide comparable values of spindle twist. Thus we use optical flow for experiments in which we test changes in the overall spindle twist in a large number of cells, and bundle tracing for experiments where high spatial precision is required.

Spindles are twisted in a left-handed manner in metaphase (Novak et al., 2018), but it is not known whether the twist is present already when the spindle assembles in prometaphase or it arises as the spindle matures. Furthermore, it is unknown how the twist changes during anaphase. To examine the development of spindle twist throughout mitosis (Fig. 1B; Movies S2-S6), we first measured twist in individual live HeLa cells expressing PRC1-GFP as they progressed through mitosis (Fig. 1C; Fig. S1C). The average twist of the spindle in prometaphase was close to 0, it was left-handed (negative) during metaphase, culminated at anaphase onset reaching a value of -1.88 ± 0.3 °/μm (n = 5), and decreased afterwards (Fig. 1C). In agreement with this result, experiments in which different spindles were imaged in different phases showed a peak of spindle twist around anaphase onset, with a value of -1.98 ± 0.26 °/μm (n = 6) (Fig. 1B, 1D; Fig. S1D-F; Movies S2-S6; Table 1).

To test whether the time spent in metaphase affects spindle twist, we accelerated entry into anaphase by inhibiting Mps1 kinase, one of the main components of the spindle assembly checkpoint (Liu and Winey, 2012). Treatment of HeLa cells expressing PRC1-GFP with the inhibitor AZ3146 (Hewitt et al., 2010) during prometaphase shortened the time to anaphase from 40 minutes to 8-10 minutes, on average. We measured the twist at the beginning of anaphase or in early anaphase and found it to be significantly smaller than in control cells, -0.17 ± 0.21 °/μm (n = 17) (Fig. S1G; Table 1). This result suggests that the reduction of time needed to enter the anaphase may also mean a reduction of time to build up spindle twist.

To explore whether spindle twist and its variation over time is specific to cancer cell lines, we measured twist in the non-cancer immortalized epithelial cell line hTERT-RPE1 (from here on referred to as RPE1) (Fig. 1B) and found that spindles in these cells also show a left-handed twist, but the values are smaller than in HeLa cells (Fig. 1E). Moreover, the temporal

pattern of twist in RPE1 cells was similar to that in HeLa cells. Twist was absent in prometaphase, it was left-handed in metaphase, had a peak value at anaphase onset, decreased during anaphase, and vanished in late anaphase (Fig. 1E; Movies S2-S6; Table 1). The value at anaphase onset was -0.53 ± 0.15 °/µm (n = 26), which indicates a weaker left-handed twist than in HeLa cells. Taken together, our results show that spindles are born without twist. The left-handed twist arises as the spindle acquires its metaphase shape, peaks at the start of chromosome segregation, and declines afterwards, both in a cancer and a non-cancer cell line.

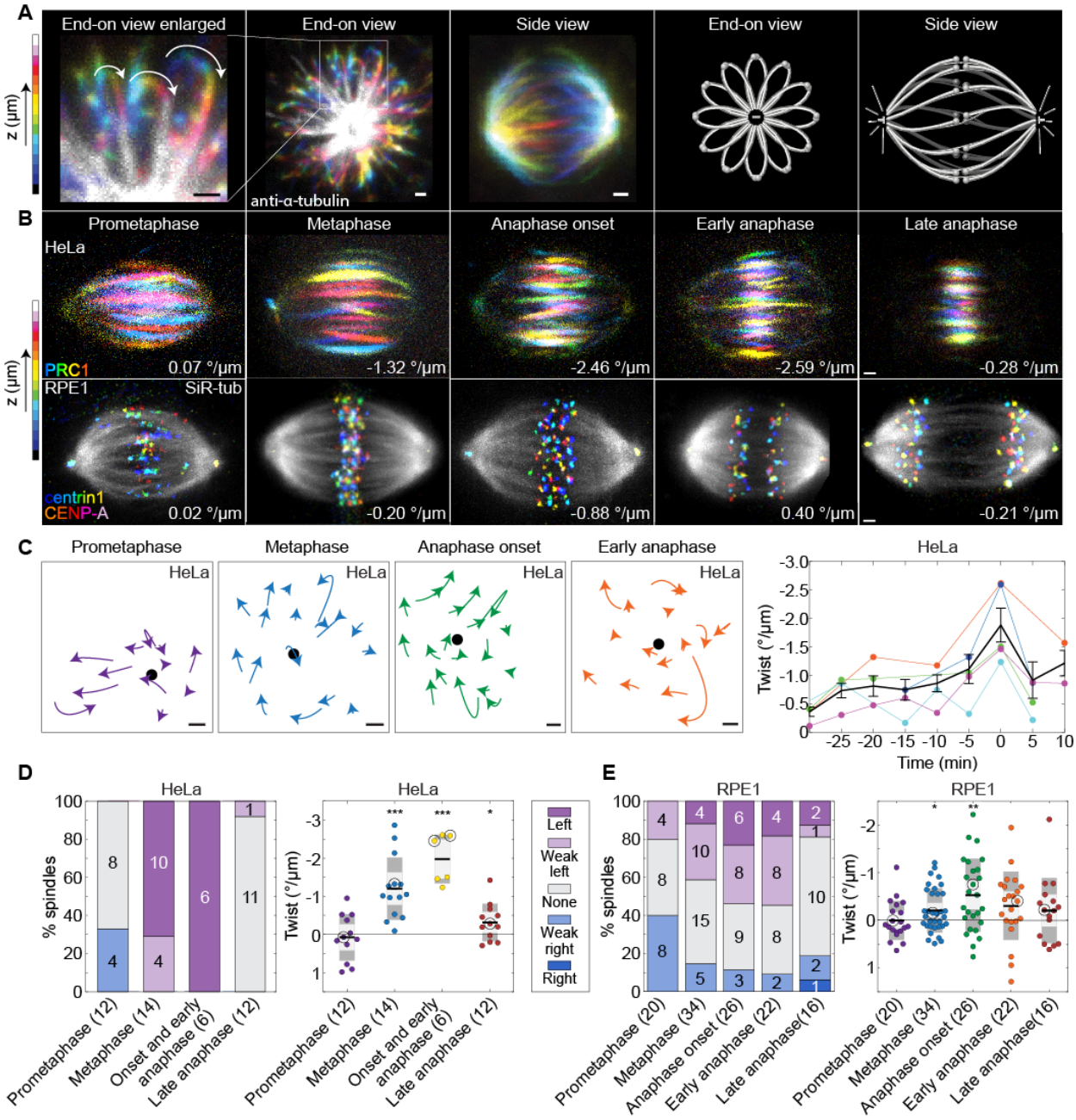

Figure 1. Spindle twist culminates at the beginning of the anaphase.

(A) Images of spindles immunostained for α-tubulin in a HeLa-Kyoto BAC cell line stably expressing PRC1-GFP (PRC1-GFP signal is not shown). Left, enlarged section of the image showing microtubule bundles from the end-on view, rotating in a clockwise direction (arrows) through z-planes when moving towards the observer. The end-on view and the side view of a spindle are shown next. Images are color-coded for depth using ImageJ temporal color coding Lookup Table '16 colors' (see color bar). Scale bar, 1 μm. Right two panels show schemes of a spindle from the end-on view and side view.

(B) Top row, images of spindles in HeLa-Kyoto BAC cells stably expressing PRC1-GFP, shown in different phases of mitosis. Bottom row, images of spindles in hTERT-RPE1 cells expressing CENP-A-GFP and centrin1-GFP, shown in different phases of mitosis. Microtubule bundles of HeLa spindles (PRC1-GFP signal) are color-coded for depth using ImageJ temporal color coding Lookup Table '16 colors' and microtubules of RPE1 spindles are shown in grey (SiR-tubulin dye) while kinetochores/centrosomes are color-coded for depth using the same color coding as described above (see color bar). Scale bars, 1 μm. Additional examples of HeLa cell spindles are shown in Fig. S1C and S1D-F.

(C) On the left, representation of microtubule bundle movements along the z-axis of the same spindle in HeLa cells viewed from the end-on view in different phases of mitosis; each microtubule bundle is represented by a circular arc of the circle fitted on the traces and arrowheads which point at the rotation direction; black dot represents the pole-to-pole axis; each color represents one phase of the mitosis; scale bar, 1 μm. On the right, graph shows the change of twist values for five HeLa cells over time; the beginning of anaphase (visible chromosome separation) was set as time zero; each color represents one cell and thick black line represents mean values with error bars showing SEM; data shown in orange originate from the cell whose bundles' movements are shown on the left and images are shown in Fig. S1C. Experiments were performed on the HeLa-Kyoto BAC cells stably expressing PRC1-GFP. Other examples of spindle images are shown in Fig. S1C.

(D) Twist in different phases of mitosis in HeLa-Kyoto BAC cells stably expressing PRC1-GFP. On the left, visual assessment graph represents percentages of spindles showing left, right, weak left, weak right or no twist, as described in the legend, in different phases of mitosis (numbers on the graph and in the brackets show the number of cells). On the right, graph shows twist values calculated with the optical flow method in different phases of mitosis. The black line shows the mean; the light and dark grey areas mark 95% confidence interval on the mean and standard deviation, respectively; ***$p<0.001$, **$p<0.01$, *$p<0.05$ (Student's t-test for the mean twist value different from 0). Circled dots represent the cells that are shown on the images above. Raw data of 10 out of 14 metaphase spindles was taken and re-calculated from (Novak et al., 2018) and also used in Fig. S1B.

(E) Twist in different phases of mitosis in hTERT-RPE1 cells expressing CENP-A-GFP and centrin1-GFP; legend as in (D).

Table 1. Spindle twist, length and width in HeLa and RPE1 cells in different phases of mitosis and after protein perturbations.

All values are shown as mean ± s.e.m; the numbers in the brackets denote the number of cells used in the analysis; n.d., not determined; * represents non-transfected HeLa cells (the rest of the data on HeLa cells comes from HeLa-Kyoto BAC cells stably expressing PRC1-GFP); RPE1 cells used were hTERT-RPE1 cells permanently transfected and stabilized using CENP-A-GFP and centrin1-GFP.

	HeLa			**RPE1**		
	Twist (°/μm)	Length (μm)	Width (μm)	Twist (°/μm)	Length (μm)	Width (μm)
Prometaphase	0.09 ± 0.18 (12)	11.8 ± 0.2	8.3 ± 0.3	0.004 ± 0.09 (20)	12.1 ± 0.2	8.7 ± 0.1
Metaphase	-1.20 ± 0.22 (14)	11.5 ± 0.3	9.0 ± 0.2	-0.21 ± 0.08 (34)	12.8 ± 0.3	9.0 ± 0.1
Anaphase onset	-1.98 ± 0.26 (6)	12.2 ± 0.4	9.0 ± 0.5	-0.53 ± 0.15 (26)	12.9 ± 0.2	8.7 ± 0.1
Early anaphase				-0.30 ± 0.15 (22)	13.8 ± 0.3	8.4 ± 0.2
Late anaphase	-0.31 ± 0.14 (12)	13.3 ± 0.2	9.0 ± 0.3	-0.20 ± 0.17 (16)	16.6 ± 0.4	7.5 ± 0.3
Mps1 inhibition	-0.17 ± 0.21 (17)	11.9 ± 0.4	8.4 ± 0.2	n.d.	n.d.	n.d.
Eg5 inhibition	-0.47 ± 0.14 (16)	12.0 ± 0.2	9.3 ± 0.2	-0.06 ± 0.19 (11)	12.3 ± 0.4	8.8 ± 0.1
Eg5 overexpression	n.d.	n.d.	n.d.	-0.25 ± 0.12 (11)	12.7 ± 0.4	9.0 ± 0.3
Kif18A siRNA	0.11 ± 0.14 (21)	12.8 ± 0.6	8.3 ± 0.2	0.28 ± 0.13 (17)	14.0 ± 0.5	8.4 ± 0.1
Kif18A overexpression	n.d.	n.d.	n.d.	-0.26 ± 0.20 (7)	10.3 ± 0.3	8.1 ± 0.2
HSET siRNA	-1.13 ± 0.21 (17)	11.7 ± 0.2	8.4 ± 0.2	-0.19 ± 0.12 (18)	13.9 ± 0.4	8.9 ± 0.1
PRC1 siRNA	*-0.94 ± 0.17 (19)	*9.9 ± 0.2	*9.9 ± 0.1	0.21 ± 0.13 (16)	15.1 ± 0.5	9.3 ± 0.2
PRC1 overexpression	n.d.	n.d.	n.d.	-0.08 ± 0.11 (10)	10.3 ± 0.4	8.0 ± 0.1
HAUS6 siRNA	0.18 ± 0.21 (16)	11.9 ± 0.3	9.4 ± 0.4	0.49 ± 0.21 (16)	11.7 ± 0.3	9.0 ± 0.1
HAUS8 siRNA	-0.35 ± 0.40 (10)	12.1 ± 0.4	9.6 ± 0.5	0.85 ± 0.24 (13)	13.1 ± 0.4	9.0 ± 0.2
Mock siRNA	*-0.85 ± 0.20 (17)	*10.7 ± 0.3	*9.6 ± 0.2	-0.22 ± 0.08 (39)	12.5 ± 0.2	8.6 ± 0.1
	-0.94 ± 0.16 (13)	11.2 ± 0.3	9.5 ± 0.3			
MG-132	n.d.	n.d.	n.d.	0.51 ± 0.14	12.0 ± 0.4	8.8 ± 0.2

Compression of the spindle along the pole-to-pole axis increases the left-handed twist

The biological role of spindle chirality is still unknown. Although chirality may be simply a side effect of the activity of torque-generating motors, the twisted shapes of microtubule bundles may contribute to spindle physiology by allowing changes of spindle shape as a passive mechanical response to external forces. To test this idea, we gently compressed vertically oriented HeLa cell spindles in metaphase along the pole-to-pole axis for 1.5 minute, following the compression protocol from a previous study (Dumont and Mitchison, 2009) (Fig. 2A; Movie S7). We used the bundle tracing method to measure spindle twist, which allowed us to graphically reconstruct spindles from the end-on view and side view (Fig. 2B). Traces of the microtubule bundles in the end-on view after 1 minute of compression were more rounded than before compression, indicating an increase in twist, and the mitotic spindle shortened (Fig. 2B). Spindle shortening was used as a measure to confirm successful compression, showing that spindle length decreased from 14.07 ± 0.55 μm before compression to 12.75 ± 0.80 μm after 1 minute of compression ($p = 0.013$; a paired t-test was used to compare the values before and after compression, $n = 6$ spindles) (Fig. 2C). Spindle width increased after compression in some cases, e.g., for the spindle shown in Fig. 2B, but overall this change was not significant ($p = 0.18$) (Fig. 2D).

Interestingly, compression resulted in a 2.3-fold increase of the left-handed spindle twist, from -0.63 ± 0.28°/μm before compression to -1.42 ± 0.50°/μm after 1 minute of compression ($p = 0.040$) (Fig. 2E; Fig. S2; Movie S7). Contour length of the microtubule bundles did not change significantly after compression ($p = 0.99$) (Fig. 2F; Fig. S2). We were unable to detect changes in bundle curvature after compression ($p = 0.41$), (Fig. 2G; Fig. S2), which is consistent with the non-significant change in spindle width. Thus, as the spindle was compressed end-on by an external force, which resulted in spindle shortening, the microtubule bundles did not shorten substantially, but instead became more twisted. These results support the idea that twist provides a passive mechanical response to force and helps the spindle to maintain integrity under load.

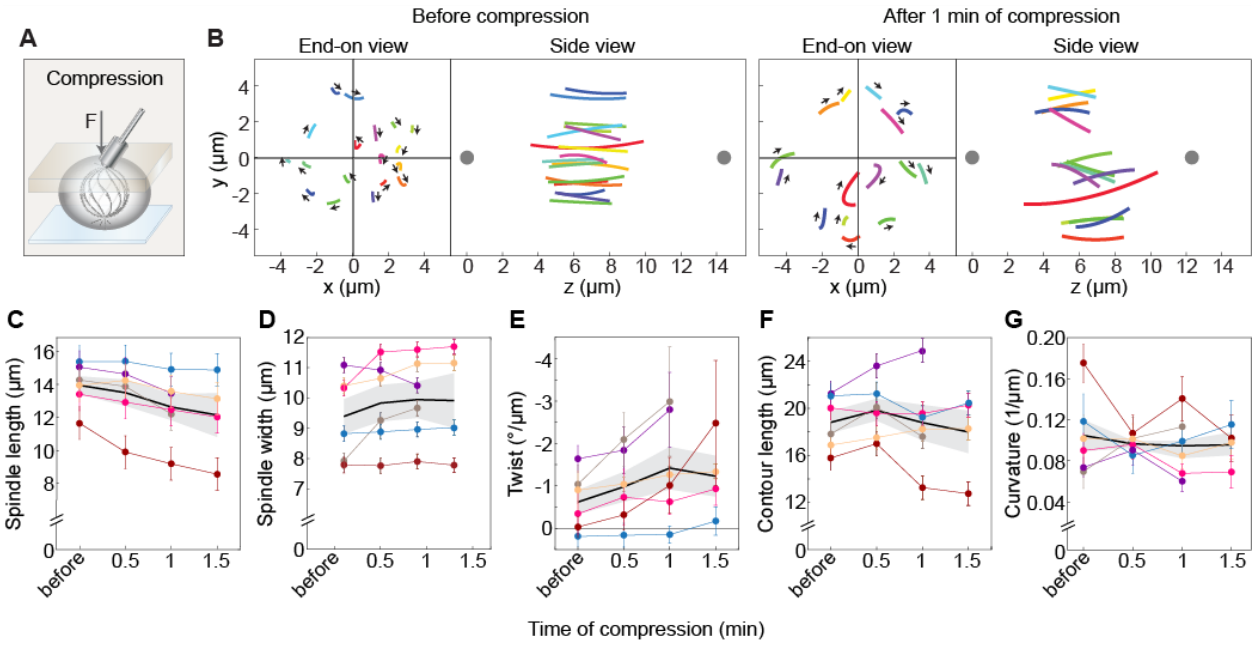

Figure 2. Spindles compressed by an external force have stronger twist.
(A) Scheme of the experimental method for spindle compression. Blue layer represents the dish; spindle is shown inside a cell with microtubule bundles in grey; grey layer represents the gel with a metal rod on top; arrow shows the direction of force.
(**B**) Microtubule bundles in a spindle shown from the end-on view and side view before compression and after 1 minute of compression, as indicated. Each bundle is represented by a different color; lines show circular arcs of the fitted circles and arrows represent the rotation direction of each bundle. Grey dots in the side view represent spindle poles.
(C)-(G) Graphs showing the change of spindle parameters from before compression up to 1.5 min of compression: spindle length **(C)**, spindle width (**D**), twist of microtubule bundles **(E)**, length of the bundle contours **(F)**, and bundle curvature **(G)**. Each color represents one cell; dots represent mean values; error bars in (C) and (D) show the estimated errors in the determination of spindle length and width, 1 µm and 0.25 µm, respectively; error bars in other graphs represent SEM. Thick black line shows the mean of all data with grey area representing SEM. Experiments were performed on the HeLa-Kyoto BAC cells stably expressing PRC1-GFP. Successful compression was performed on 6 spindles from 5 independent experiments. Individual data points are shown in Fig. S2.

Motor proteins Eg5/kinesin-5 and Kif18A/kinesin-8 regulate spindle twist

To explore the molecular origins of torques in the spindle and thus its twisted shape, we consider the following molecular activities. First, motors that exert torque on the microtubule may generate the twisted shape of the bundle by twisting the microtubules within the bundle around each other, or by twisting the microtubules with respect to the spindle pole. Second, proteins that crosslink neighboring microtubules or link microtubules with the pole may prevent free rotation

of the microtubules, thereby allowing for twisting of the bundles. Third, nucleation of new microtubules within the bundle may affect the bundle twist.

To test the role of these activities in the regulation of spindle twist, we performed a candidate screen on HeLa and RPE1 cells in which we perturbed motor proteins and other microtubule-associated proteins one by one using siRNA-mediated depletion, small-molecule inhibitors, or overexpression, and measured the resulting spindle twist. As the candidates for this mini-screen, we selected spindle-localized motor proteins for which it has been shown *in vitro* that they can rotate the microtubule (Eg5/kinesin-5, Kif18A/ kinesin-8, HSET/kinesin-14), the main crosslinker of antiparallel microtubules PRC1, and the augmin complex that is responsible for the nucleation of microtubules along existing microtubules. Spindle twist was measured during metaphase, rather than at anaphase onset when twist is most pronounced, because depletion of Kif18A or augmin interferes with anaphase entry (Stumpff et al., 2008; Uehara et al., 2009). Depletion of each protein was confirmed by measurements of the immunofluorescence signal of that protein on the spindle (Fig. S3).

In agreement with our previous work on HeLa cells (Novak et al., 2018), we found that inhibition of Eg5 with S-trityl-L-cysteine (STLC) decreased spindle twist in HeLa and abolished twist in RPE1 cells (Fig. 3A, 3B, 3C; Fig. S4, S5; Table 1). Depletion of Kif18A abolished spindle twist in HeLa cells and resulted in right-handed twist in RPE1 cells, causing ~65% of RPE1 spindles to twist in the right-handed fashion (Fig. 3A, 3B, 3C; Fig. S4, S5; Movie S8; Table 1). Overexpression of either Eg5 or Kif18A in RPE1 cells did not yield any changes in twist (Fig. 3C; Fig. S5; Table 1). Depletion of HSET/kinesin-14 did not change twist in HeLa or RPE1 cells (Fig. 3A, 3B, 3C; Fig. S4, S5; Table 1). We conclude that Eg5 and Kif18A regulate the torques within the spindle, which lead to the twisted shape of microtubule bundles (Fig. 3A, schemes).

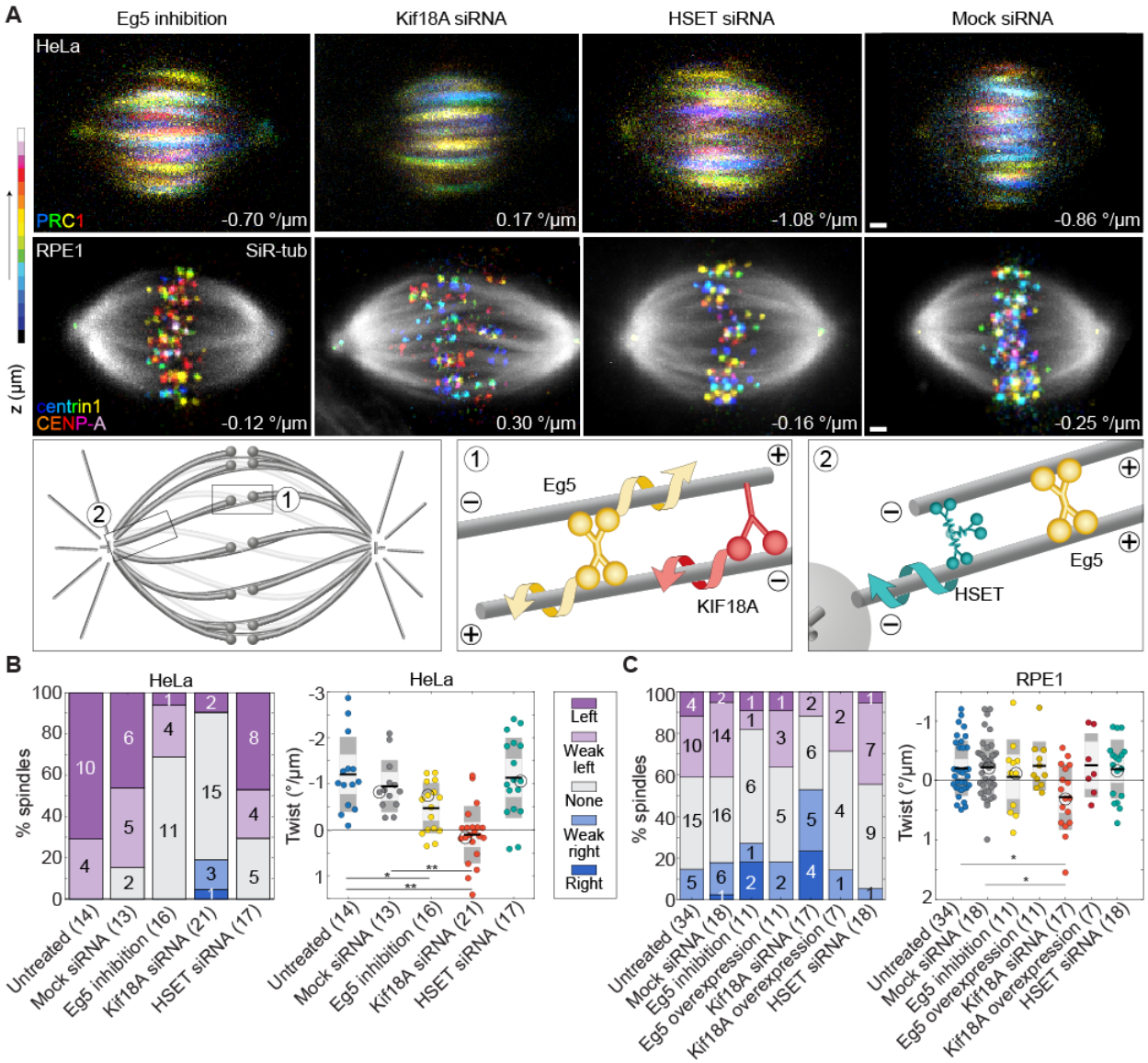

Figure 3. Motor proteins Eg5 and Kif18A control spindle twist.

(A) First row, images of the spindles in HeLa-Kyoto BAC cells stably expressing PRC1-GFP after inhibition/depletion of Eg5, Kif18A and HSET motor proteins. Second row, images of the spindles in hTERT-RPE1 cells permanently transfected and stabilized using CENP-A-GFP and centrin1-GFP after inhibition/depletion of Eg5, Kif18A and HSET motor proteins. Third row, simplified schemes showing localization and movement of Eg5, Kif18A and HSET motor proteins in the spindle. Microtubule bundles of HeLa spindles (PRC1-GFP signal) are color-coded for depth using ImageJ temporal color coding Lookup Table '16 colors' and microtubules of RPE1 spindles are shown in grey (SiR-tubulin dye) while kinetochores/centrosomes are color-coded for depth using the same color coding as described above (see color bar). Scale bars, 1 µm. Additional examples of spindles are shown in Figs. S4, S5.

(B) Spindle twist after perturbations of motor proteins in HeLa cells expressing PRC1-GFP. Left, visual assessment graph represents percentages of spindles showing left, right, weak left, weak right or no twist, as described in the legend, after inhibition/depletion of Eg5, Kif18A and HSET (numbers on the graph

and in the brackets show the number of cells). Right, graph shows twist values calculated with the optical flow method after inhibition/depletion of Eg5, Kif18A and HSET motor proteins. The black line shows the mean; the light and dark grey areas mark 95% confidence interval on the mean and standard deviation, respectively; one-way ANOVA test showed significant difference between group means ($p = 3.16 \times 10^{-7}$); *p<0.05, **p<0.01 (Tukey's HSD post hoc test); significant difference between Kif18A siRNA and HSET siRNA is not shown on the graph (**p<0.01). Circled dots represent cells that are shown on the images above.

(C) Spindle twist after perturbations of motor proteins in RPE1 cells expressing CENP-A-GFP and centrin1-GFP; legend as in (B). One-way ANOVA test showed significant difference between group means (p = 0.02); *p<0.05 (Tukey's HSD post hoc test).

Depletion of PRC1 makes RPE1 spindles twist in a right-handed manner, whereas overexpression of PRC1 abolishes twist

PRC1 protein is a key regulator of cytokinesis (Jiang et al., 1998), but also the main crosslinking protein of antiparallel microtubules within bridging fibers (Kajtez et al., 2016; Polak et al., 2017). Without PRC1, bridging fibers are thinner and spindles have less curved and more diamond-like shape (Jagric et al., 2021; Kajtez et al., 2016), which led us to hypothesize that the twist might also be affected. In HeLa cells, depletion of PRC1 did not yield changes in the spindle twist (Fig. 4A, 4B; Fig. S4; Movie S9; Table 1), but, surprisingly, when we depleted PRC1 in RPE1 cells, the spindles had right-handed twist of 0.21 ± 0.13 °/μm (n = 16) (Fig. 4A, 4C; Fig. S5; Movie S9; Table 1). In contrast, overexpression of PRC1 in RPE1 cells resulted in the abolishment of the spindle twist, with a complete lack of rotational movement of microtubule bundles (Fig. 4A, 4C; Fig. S5; Movie S9; Table 1). Taken together, these data suggest that PRC1 regulates torques within the spindle in RPE1 cells, possibly by limiting free rotation of microtubules within antiparallel bundles.

Depletion of augmin leads to zero twist in HeLa cells and right-handed twist in RPE1 cells

The augmin complex is responsible for the microtubule nucleation from the lateral surface of the pre-existing microtubules (David et al., 2019; Uehara et al., 2009). Augmin is important for the nucleation of the bridging fibers and, consequentially, the maintenance of the spindle shape (Manenica et al., 2020). When we depleted the augmin subunit HAUS6, the spindles in HeLa cells had zero twist on average, whereas those is RPE1 cells had right-handed twist of 0.49 ± 0.21 °/μm (n = 16) (Fig. 4A, 4B, 4C; Fig. S4, S5; Table 1). A similar result was observed after the depletion of the augmin subunit HAUS8, which resulted in zero average twist in HeLa cells and a strong right-handed twist in RPE1 cells of 0.85 ± 0.24 °/μm (n = 13) (Fig. 4A, 4B, 4C; Fig. S4, S5; Movie S10; Table 1). Thus, augmin-mediated nucleation of microtubules along the wall

of pre-existing microtubules is an important determinant of the direction and amount of spindle twist.

As depletion of the augmin complex subunits prolongs metaphase (Uehara et al., 2009), we explored how the twist changes when cells are arrested in metaphase by adding the proteasome inhibitor MG-132. Interestingly, spindles in RPE1 cells arrested in metaphase had right-handed twist of 0.51 ± 0.14 °/µm (n = 15) (Fig. 4C; Table 1), suggesting that prolonging metaphase may cause a shift in the balance of torque-generating activities resulting in a right-handed twist.

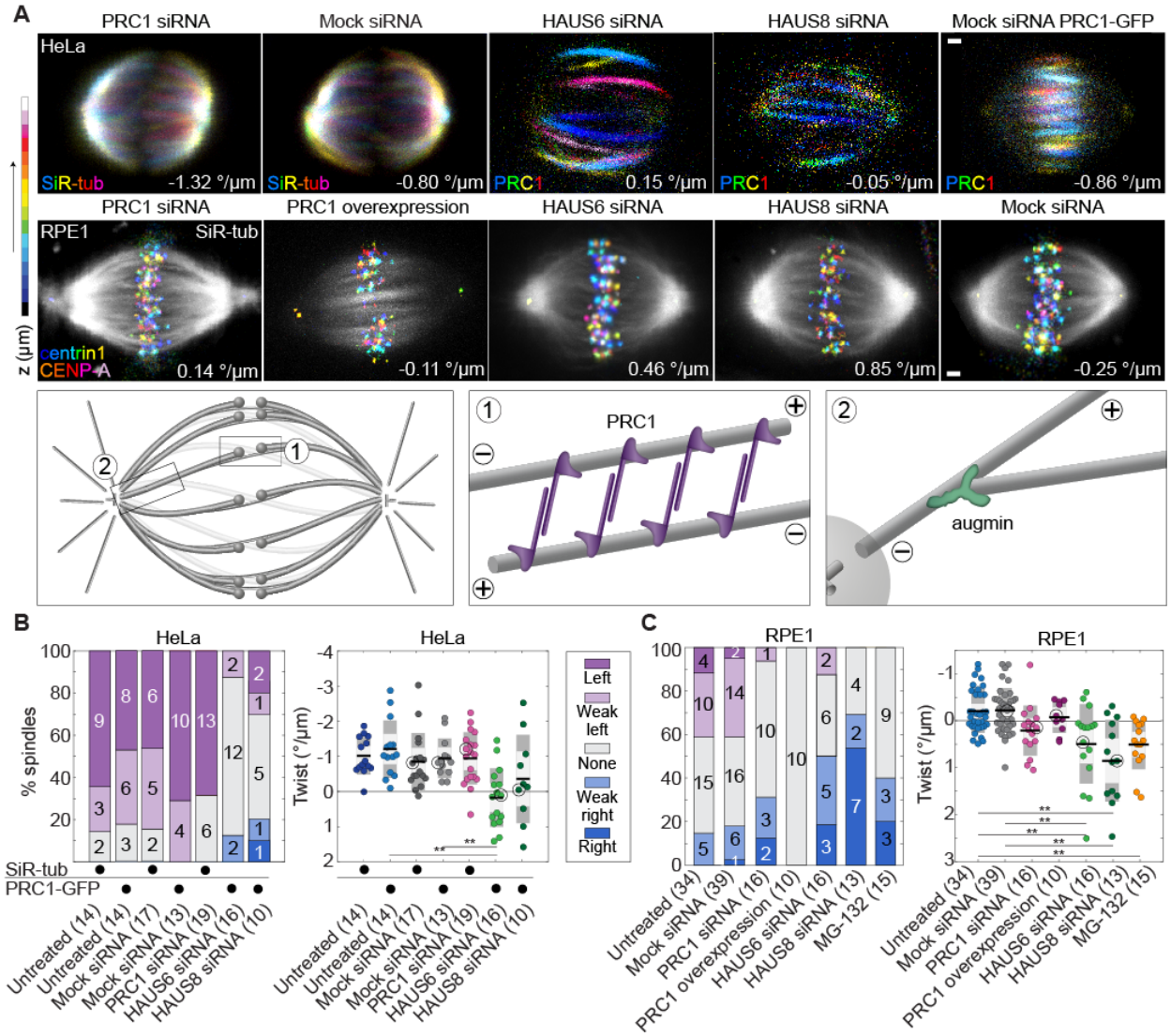

Figure 4. Microtubule crosslinker PRC1 and nucleator augmin regulate spindle twist.

(A) First row, images of spindles in a non-transfected HeLa cell line stained with SiR-tubulin (first 2 spindles) and HeLa-Kyoto BAC cells stably expressing PRC1-GFP (last 3 spindles), after depletion of

PRC1 and subunits of the augmin complex HAUS6 and HAUS8. Second row, images of spindles in the hTERT-RPE1 cells, permanently transfected and stabilized using CENP-A-GFP and centrin1-GFP RPE1, after perturbations of PRC1 and depletions of subunits of the augmin complex HAUS6 and HAUS8. Third row, simplified schemes showing the localization of PRC1 and augmin in the spindle. Microtubule bundles in HeLa cells (PRC1-GFP signal in HeLa-Kyoto BAC cells and SiR-tubulin dye in non-transfected HeLa cells) are color-coded for depth using ImageJ temporal color coding Lookup Table '16 colors' and microtubules of RPE1 spindles are shown in grey (SiR-tubulin dye, except the cells with overexpressed PRC1 that show PRC1-mCherry signal), while kinetochores/centrosomes are color-coded for depth using the same color coding as described above (see color bar). Scale bars, 1 μm. Additional examples of spindles are shown in Fig. S4, S5.

(B) Spindle twist after perturbations of PRC1 and augmin in HeLa cells. Left, visual assessment graph represents percentages of spindles showing left, right, weak left, weak right or none twist, as described in the legend, after depletions of PRC1 protein and subunits of augmin complex HAUS6 and HAUS8 in HeLa cells (numbers on the graph and in the brackets show the number of cells; black dots under the graph denote the cell line/staining used for the corresponding treatment). Right, graph shows twist values calculated with the optical flow method after depletions of PRC1 protein and subunits of augmin complex HAUS6 and HAUS8. The black line shows the mean; the light and dark grey areas mark 95% confidence interval on the mean and standard deviation, respectively; one-way ANOVA test showed significant difference between group means ($p = 8.06 \times 10^{-5}$); $^{**}p<0.01$ (Tukey's HSD post hoc test). Circled dots represent cells that are shown on images. Experiments were performed on the non-transfected HeLa cell line (for the depletion of PRC1 and its control) and HeLa-Kyoto BAC cells stably expressing PRC1-GFP (for the depletion of the HAUS6 and HAUS8 and their controls).

(C) Spindle twist after perturbations of PRC1 and augmin in RPE1 cells expressing CENP-A-GFP and centrin1-GFP; legend as in (B). One-way ANOVA test showed significant difference between group means ($p = 2.49 \times 10^{-9}$); $^{**}p<0.01$ (Tukey's HSD post hoc test); significant differences between HAUS8 siRNA with PRC1 overexpression ($^{**}p<0.01$) and PRC1 siRNA ($^{*}p<0.05$) are not shown on the graph.

Round spindles are more twisted than elongated spindles

While imaging different types of spindles (phases of mitosis, cell lines, protein perturbation), we noticed that round spindles generally have stronger twist than elongated spindles. In order to quantify this observation, we measured spindle length and width and calculated the width/length ratio as a measure for the roundness of the spindle, where ratios closer to 1 describe round spindles, and smaller values elongated spindles (Fig. 5A, scheme). Higher width/length ratios are a signature of stronger bending moments in the spindle (Novak et al., 2018). We tested the correlation between the width/length ratios and twist values in metaphase, and found that in non-transfected HeLa cells, whose width/length ratios were roughly between 0.8 and 1, rounder spindles had a stronger left-handed twist (Fig. 5A). In contrast, no correlation was observed in RPE1 cells, whose width/length ratios were between 0.5 and 0.8 (Fig. 5A). A weak correlation was found in HeLa cells expressing PRC1-GFP, which had smaller width/length ratios than non-

transfected HeLa cells (Fig. S6A). Overall, twist was correlated with roundness among spindles with width/length ratios above ~0.8, suggesting a correlation between twist and bending moments.

A plot of the twist as a function of the width/length ratio for various mitotic phases and treatments indicates that different combinations of twist and bending moments exist in spindles in different phases of mitosis or in which different molecular mechanisms are perturbed (Fig 5B, 5C; see Fig. S6 for twist vs. width or length). In HeLa cells, prometaphase and late anaphase spindles are elongated with zero and small left-handed twist values, respectively (Fig. 5B). Left-handed twist rises during metaphase when spindles are the roundest, and highest twist values are at the beginning of anaphase when spindles are still rather round (Fig. 5B). In contrast, in RPE1 cells such correlation between twist and roundness over mitotic phases was not observed (Fig. 5B). These observations suggest that roundness and twist are correlated over mitotic phases for spindles that have a high width/length ratio (above ~0.7; Fig. 5B), which is in agreement with the correlation among individual metaphase cells (Fig. 5A).

In HeLa cells, left-handed twist was predominantly found in spindles with mild or high width/length ratios, whereas right-handed twist was found in spindles with lower width/length ratios (Fig. 5B, 5C). In RPE1 cells, both left-handed and right-handed twist was found in spindles over the whole range of width/length ratios (Fig. 5B, 5C). Taken together, these results suggest that spindles with more round shapes are made of bundles that are more twisted in the left-handed direction than spindles with elongated shapes.

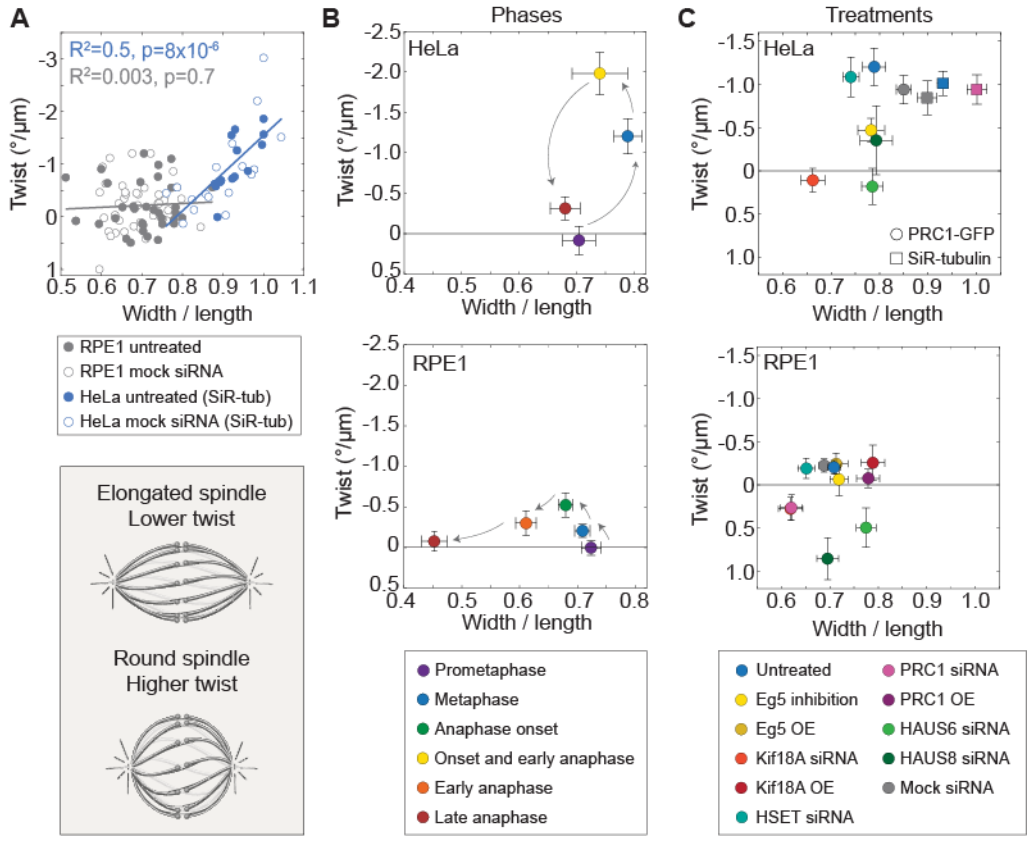

Figure 5. Round spindles have stronger twist than elongated spindles.

(A) Graph shows the correlation between width/length ratio and twist in HeLa and RPE1 cells. Filled circles represent untreated cells while empty circles represent mock siRNA controls as indicated in the legend below the graph. Lines show linear fits for each cell line (untreated cells together with mock siRNA controls); equations y=-7.16x+5.62 for non-transfected HeLa cells and y=-0.36x+0.04 for RPE1 cells; goodness of fit is shown in the graph. Data for HeLa cells were also used in graphs in Fig. 4B. Data for RPE1 cells were also used in graphs in Figs. 1E, 3C, 4C. Experiments were performed on the non-transfected HeLa cell line and hTERT-RPE1 cells, permanently transfected and stabilized using CENP-A-GFP and centrin1-GFP. The scheme on the bottom shows that elongated and round spindles, with lower and higher width/length ratio, have lower and higher twist, respectively.

(B) Graphs showing how the spindle twist and width/length ratio in HeLa (top) and RPE1 cells (bottom) vary over different phases of mitosis. Each color represents a phase, as described in the legend below the graphs; error bars represent SEM; arrows indicate progression of mitosis. The same data were used in graph in Figs. 1D, 1E. Experiments were performed on the HeLa-Kyoto BAC cells stably expressing PRC1-GFP and hTERT-RPE1 cells permanently transfected and stabilized using CENP-A-GFP and centrin1-GFP.

(C) Graphs showing how the spindle twist and width/length ratio in HeLa (top) and RPE1 cells (bottom) vary depending on the perturbations of spindle-associated proteins. Colors represent different protein perturbation, as described in the legend below the graphs; error bars represent SEM. The same data were used in graphs in Figs. 3B, 3C, 4B, 4C. For HeLa cells, experiments were performed on HeLa-Kyoto

BAC cells stably expressing PRC1-GFP (circles) and non-transfected HeLa cells stained with SiR-tubulin (rectangles), and hTERT-RPE1 cells permanently transfected and stabilized using CENP-A-GFP and centrin1-GFP.

DISCUSSION

Mechanisms that generate spindle twist

The chiral shape of the human mitotic spindle, visible as the left-handed twist of microtubule bundles, implies that torques act within the spindle. In this work we reveal biomechanical and molecular mechanisms that regulate the torques within microtubule bundles reflected in the spindle twist. From a biomechanical point of view, we show that forces within or outside the spindle regulate spindle twist (Fig. 6A, box 1). We found that among the spindles in HeLa cells, which show different shapes during metaphase, round spindles are more twisted than elongated ones. In agreement with this, spindles in metaphase and just after anaphase onset are more round and more twisted than in prometaphase and late anaphase, when the spindles are elongated and twist is largely absent. In RPE1 spindles, which are overall more elongated than HeLa spindles, twist is weaker. Moreover, when we squeezed HeLa spindles along the pole-to-pole axis, they became more round and their twist increased. These findings suggest that spindle roundness, which reflects bending moments within the spindle (Novak et al., 2018), is correlated with twist. Thus, the molecular mechanisms that generate larger bending moments, causing the spindles to be rounder, may also generate larger twisting moments, visible as stronger twist of the microtubule bundles.

We hypothesized that the torques within the bundles are generated by motor proteins, especially those that step in a chiral manner. By performing a candidate screen in which we perturbed motor proteins and other microtubule-associated proteins, we identified several molecular players involved in the regulation of spindle chirality, suggesting that spindle twist is controlled by multiple mechanisms acting at different locations within the spindle. Inactivation of Eg5 decreased the left-handed twist in HeLa cells (Novak et al., 2018) and led to zero twist in RPE1 cells, whereas depletion of Kif18A resulted in zero twist in HeLa cells and a switch of the twist direction from left-handed to right-handed in RPE1 cells. Overexpression of these proteins did not change the twist. Both of these motors are known to exert torque on the microtubules *in vitro* (Bormuth et al., 2012; Mitra et al., 2018; Yajima et al., 2008), and are found within the antiparallel overlaps of bridging microtubules in the spindle (Jagric et al., 2021; Kajtez et al., 2016; Mann and Wadsworth, 2018). Thus, we suggest that they generate the twisted shape of the bundle by rotating the antiparallel microtubules within the bundle around each other (Fig. 6A, box 2). Eg5 may also contribute to spindle twist by acting at the spindle pole (Fig. 6A, box 3), given that the most pronounced localization of Eg5 is in the pole region (Kajtez et al., 2016;

Mann and Wadsworth, 2018). Here, Eg5 may crosslink parallel microtubules (Valentine et al., 2006; Walczak et al., 1998), which would prevent their free rotation within the bundle and promote the accumulation of torsional stresses. Additionally, other motors localized at the pole may contribute to spindle twist by rotating the microtubules with respect to the spindle pole (Fig. 6A, box 3).

Intriguingly, the strongest effect on spindle twist was obtained by depletion of the HAUS6 and HAUS8 subunits of the augmin complex, which promotes nucleation of new microtubules from the wall of existing microtubules (David et al., 2019; Goshima et al., 2008; Uehara et al., 2009). These depletions resulted in zero twist in HeLa cells and right-handed twist in RPE1 cells. How could augmin regulate the twist of microtubule bundles? Augmin depletion results in a substantial reduction of the microtubule number within bridging fibers (Manenica et al., 2020), which may affect the twist by reducing the antiparallel overlaps where torque-generating motors such as Eg5 and Kif18A bind (Fig. 6A, box 2). In addition, augmin nucleates new microtubules at an angle with respect to the wall of the old microtubule (Kamasaki et al., 2013; Petry et al., 2013), thus it is tempting to speculate that if the new microtubules extend skewed from the old microtubules and spiral around them, this may lead to the twist of the entire microtubule bundle.

Similarly to augmin perturbation, depletion of the crosslinker of antiparallel microtubules PRC1 led to right-handed twist in RPE1 cells. We propose that in a metaphase spindle the microtubules crosslinked by PRC1 cannot rotate freely within the bundle, resulting in the accumulation of torsional stresses (Fig. 6A, box 2). Yet the torsional rigidity of the whole bundle is low enough to allow for twisting of the bundle. In contrast, in late anaphase, when PRC1 is highly abundant on midzone microtubules, and in experiments with PRC1 overexpression in metaphase, the bundles had completely straight shapes. The high amount of PRC1 within the bundles may result in an increased number of bundled microtubules, which in turn increases the torsional rigidity of the bundle making it harder to twist.

Duration of metaphase also affects the spindle twist. Arresting RPE1 cells in metaphase resulted in right-handed twist, similar to the depletion of Kif18A or the augmin complex. Interestingly, these depletions also prolong metaphase (Stumpff et al., 2008; Uehara et al., 2009), which may contribute to the observed effect on twist.

The switch of the direction of twist from left-handed to right-handed indicates the existence of competing mechanisms promoting twist in the opposite directions. Different perturbations may tip the balance one way or the other. HeLa spindles have stronger left-handed twist than RPE1 spindles, and protein depletions that led to zero twist in HeLa cells largely resulted in right-handed twist in RPE1 cells, thus the twist changed in both cell lines by a similar amount. This implies that torques are regulated by similar mechanisms in both cell lines, but the torque balance is shifted more towards the formation of left-handed twist in HeLa than in RPE1 spindles. Unlike metaphase, in anaphase twist is mostly absent in HeLa and RPE1 spindles. A recent study found strong left-handed twist during anaphase after combined Eg5 inhibition and

NuMa depletion in RPE1 cells, suggesting that opposing motors are required to prevent twisting in the anaphase spindle (Neahring et al., 2021).

In contrast to the left-handed twist of human spindles, spindles in the amoeba *Naegleria gruberi* are twisted in a right-handed fashion (Velle et al., 2021), which may be due to the differences in kinesins and other microtubule-associated proteins between *Naegleria* and humans. What determines the direction and amount of twist in spindles of different organisms remains an intriguing topic for future studies.

Physiological function of spindle twist

Although spindle chirality may be simply a side-effect of the action of motors that generate torque, the twisted shapes of microtubule bundles may contribute to spindle function. We propose that the twisted shape observed during metaphase is beneficial for the spindle because it allows for changes of spindle shape as a passive mechanical response to external forces. In this picture, a twisted spindle can quickly shorten under compressive forces by passively increasing the twist in a manner similar to an elastic spring (Fig. 6B, top). This response does not require depolymerization of microtubules during spindle shortening, which would be the case for non-twisted spindles. Our experiments in which we compressed the spindle along the pole-to-pole axis and observed an increase in twist as the spindle shortened, while the contour length of microtubule bundles remained largely unchanged, provide support for the model in which the built-in twist helps the spindle to respond to forces and decreases the risk of spindle breakage under high load.

In contrast to metaphase, during late anaphase, the spindle is not chiral as the bundles lose their twist and become straight. This straightening is likely due to the accumulation of PRC1 and also other midzone proteins within these bundles. We speculate that the straight shapes of the bundles are beneficial for the spindle in late anaphase to make the spindle mechanically robust and keep the chromosomes well separated (Fig. 6B, bottom).

Additional functions of spindle chirality may be to promote physical separation of adjacent bundles during prometaphase or to help start spindle elongation at the onset of anaphase, which await further explorations. Overall, we expect that the results presented here will motivate exciting new research on the molecular mechanisms and the biological roles of rotational forces in the spindle.

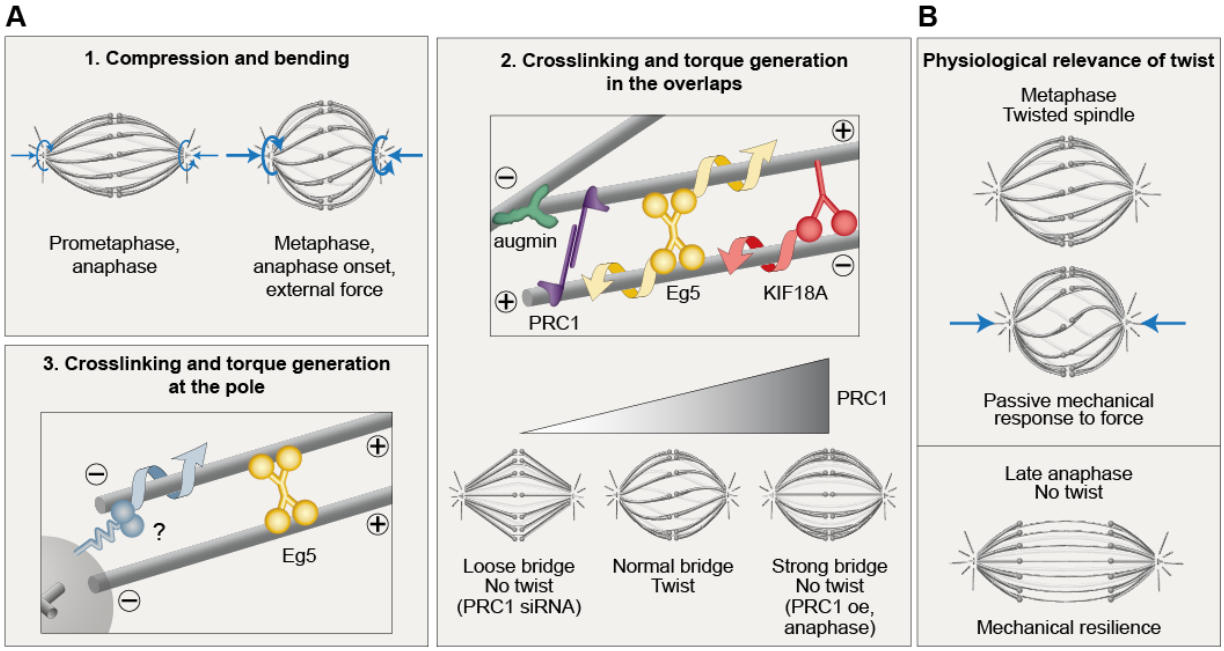

Figure 6. Biomechanical and molecular origins of spindle twist and its biological role.
(A) Forces regulate twist (box 1). Round spindles or those compressed by external forces (blue straight arrows) are more twisted than elongated ones, suggesting that larger bending moments (blue curved arrows) are correlated with larger twist. Within the antiparallel overlaps of bridging microtubules (box 2), Eg5 and Kif18A rotate the microtubules around one another, whereas crosslinking by PRC1 constrains the free rotation of microtubules within the bundle, allowing for accumulation of torsional stresses (the triangle represents the amount of PRC1, oe stands for overexpression). Augmin contributes to the twist by nucleating bridging microtubules. At the spindle pole (box 3), Eg5 crosslinks parallel microtubules, which may prevent their free rotation, and other motors may rotate the microtubules around the pole.
(B) Spindle twist allows for a passive mechanical response to external forces during metaphase (top). In contrast, in late anaphase twist is absent, which promotes spindle rigidity and maintenance of chromosome separation (bottom).

MATERIALS AND METHODS

Cell lines

Experiments were performed using: HeLa-Kyoto BAC cell line stably expressing PRC1-GFP courtesy of Ina Poser and Tony Hyman (Max Planck Institute of Molecular Cell Biology and Genetics, Dresden, Germany); unlabeled (non-transfected) HeLa-TDS cells from the High-Throughput Technology Development Studio (MPI-CBG, Dresden); human hTERT-RPE1 permanently transfected and stabilized using CENP-A-GFP and centrin1-GFP courtesy of Alexey Khodjakov (Wadsworth Center, New York State Department of Health, Albany, NY). Cells were grown in flasks in Dulbecco's modified Eagle's medium (DMEM; Capricorn Scientific GmbH, Germany) supplemented with 10% fetal bovine serum (FBS; Sigma-Aldrich, MO, USA), 10000 U/ml penicillin/streptomycin solution (Capricorn Scientific GmbH, Germany), and for HeLa-Kyoto BAC cells also 50 µg/mL geneticin (Life Technologies, Waltham, MA, USA). The cells were kept at 37°C and 5% CO2 in a Galaxy 170S CO2 humidified incubator (Eppendorf, Hamburg, Germany) and regularly passaged at the confluence of 70-80%.

Sample preparation

To visualize microtubules in experiments on RPE1 and unlabelled HeLa cells, silicon rhodamine (SiR)-tubulin (λ_{Abs} 652 nm, λ_{Em} 674 nm) (Spirochrome AG, Stein am Rhein, Switzerland) dye was added to the dish at the final concentration of 100 nM, 2-3 hours prior to imaging. To visualize chromosomes and determine phase of the mitosis of the spindle in experiments on HeLa PRC1-GFP cells, 1 h prior to imaging silicon rhodamine (SiR)-DNA (λ_{Abs} 652 nm, λ_{Em} 674 nm) (Spirochrome AG, Stein am Rhein, Switzerland) was added to the dish at a final concentration of 100 nM. Lipofectamine RNAiMAX reagent (Invitrogen by Thermo Fisher Scientific, MA, USA) was used for RNAi treatments following manufacturer's instructions. Transfections with siRNA were always performed 48h prior to imaging at the final concentration of 100 nM. For the inhibition of Eg5, cells were treated with (+)-S-Trityl-L-cysteine (STLC, Sigma-Aldrich, MO, USA) at the final concentration of 40 µM right before the imaging so that cells are not yet collapsed into a monopol during imaging. For depletion of endogenous Kif18A, cells were transfected with Kif18A Silencer Select siRNA (4390825, Ambion, Thermo Fisher Scientific, MA, USA). In mock experiments cells were transfected with equal amount of Silencer Select Negative Control #1 siRNA (4390843, Ambion, Thermo Fisher Scientific, MA, USA). For depletion of endogenous PRC1, cells were transfected with ON-TARGETplus SMARTpool Human PRC1 (L-C19491-00-0010, Dharmacon, CO, USA). For depletions of endogenous HAUS6 and HAUS8, cells were transfected with ON-TARGETplus SMARTpool Human HAUS6 (L-018372-01-0005, Dharmacon, CO, USA) and ON-TARGETplus SMARTpool Human HAUS8 (L-031247-01-0005, Dharmacon, Co, USA), respectively. For the depletion of endogenous HSET, cells were transfected with ON-TARGETplus SMART pool Human KIFC1

(L-004958-00, Dharmacon, CO, USA). In mock experiments cells were transfected with equal amount of ON-TARGETplus Control Pool Non-Targeting pool (D-001810-10-05, Dharmacon, CO, USA). All plasmid transfections were performed using Nucleofactor Kit R with the Nucleofactor 2b Device (Lonza, Basel, Switzerland) using Y-001 program for human HMEC cells (high efficiency). To overexpress Eg5 protein, cells were transfected with 5 μg of mEmerald-Kinesin11-N-18 plasmid (Addgene number: 54137) 24h prior to imaging. For Kif18A overexpression, cells were transfected with 5 μm of EGFP-Kif18A plasmid that was a gift from Jason Stumpff (University of Vermont, Burlington, VT, USA). To overexpress PRC1 protein, cells were transfected with 5 μg of mCherry-PRC1 plasmid that was a gift from Casper C. Hoogenraad (Utrecht University, Utrecht, Netherlands). To reduce the time in which HeLa cells reach anaphase, the Mps1 inhibitor AZ3146 (Sigma-Aldrich, MO, USA) was added in prometaphase at a final concentration of 4 μM. Metaphase arrest in RPE1 cells was performed with the proteasome inhibitor MG-132 (M7449, Sigma-Aldrich, MO, USA) added at least two hours prior to imaging at a final concentration of 20 μM. All experiments were performed at least three times in both cell lines, except Kif18A overexpression that was preformed once. To prepare samples for microscopy, RPE1 and HeLa cells were seeded and cultured in DMEM medium with supplements at 37°C and 5% CO2 on uncoated 35-mm glass coverslip dishes with 0.17-mm (1.5 coverglass) glass thickness (MatTek Corporation, Ashland, MA, USA).

Immunofluorescence

HeLa-Kyoto BAC cell line stably expressing PRC1-GFP were grown on glass-bottomed dishes (14 mm, No. 1.5, MatTek Corporation) and fixed by a microtubule-preserving mixture of 3.2% PFA (paraformaldehyde) and 0.25% GA (glutaraldehyde) in microtubule-stabilizing PEM buffer (0.1 M PIPES, 0.001 M $MgCl_2$ x 6 H_2O, 0.001 M EDTA, 0.5 % Triton-X-100) for 10 min at room temperature. After fixation with PFA and GA, for quenching, cells were incubated in 1mL of freshly prepared 0.1% borohydride in PBS (phosphate-buffered saline) for 7 min and after that in 1 mL of 100 mM NH_4Cl and 100 mM glycine in PBS for 10 min at room temperature. Cells were then washed with 1 mL of PBS, 3 times for 5 min. To block unspecific binding of antibodies, cells were incubated in 500 μL blocking/permeabilization buffer (2% normal goat serum (NGS) and 0.5% Triton-X-100 in water) for 45 min at room temperature. Cells were then incubated in 500 μL of primary antibody solution (rat anti-alpha Tubulin YL1/2 (MA1-80017, Invitrogen, CA, SAD), diluted 1:500) for 24h at 4°C. After primary antibody, cells were washed in PBS and then incubated in 500 μL of secondary antibody solution (donkey anti-rat IgG Alexa Fluor 594 (ab150156, Abcam), diluted 1:1000) for 45 min at room temperature.

Human hTERT-RPE1 cells, permanently transfected and stabilized using CENP-A-GFP and centrin1-GFP, were grown on glass-bottomed dishes (as described above) and fixed in cold 100% methanol for 1 min on the ice block. After fixation, cells were washed in PBS 3 times for 5 min at room temperature. Next, cells were additionally permeabilized in 0.5% Triton-X-100 solution for 15 min at room temperature and then washed in PBS (as described above). To block

unspecific binding of antibodies, cells were incubated in 1% NGS solution for 1h on 4°C. After washing in PBS once, cells were incubated with primary antibodies (dilution 1:100 in 1% NGS) overnight on 4°C. Next, cells were washed in PBS 3 times for 5 min at room temperature and incubated with secondary antibodies (dilution 1:250 in 2% NGS solution) for 1h at room temperature covered with aluminum foil. Before microscopy, cells were washed in PBS (as described above) and left in PBS during imaging. Cells were kept in the dark in PBS on 4°C. Primary antibodies used: PRC1 (C-1) mouse monoclonal IgG_1 (sc-376983, Santa Cruz Biotechnology, TX, USA), Rabbit anti-KIF18A Affinity Purified (A301-080A, Bethyl, TX, USA), Rb pAb to FAM29A (ab150806, Abcam, Cambridge, UK), HICE1 Polyclonal Antibody (PA5-21331, Invitrogen, MA, USA), KIFC1 (M-63) mouse monoclonal IgG_{2a} (sc-100947, Santa Cruz Biotechnology, TX, USA); secondary antibodies used: Dnk pAb to Ms IgG (ab150112, Abcam, Cambridge, UK), Dnk pAb to Rb IgG (ab150064, Abcam, Cambridge, UK).

Spindle compression

Spindle compression method was optimized from Mitchison and Dumont, 2009 (Dumont and Mitchison, 2009). A solution of 2 % ultra-pure agarose (15510 Invitrogen by Thermo Fisher Scientific, MA, USA) in PBS was prepared, brought to boil and 2 ml was put in a 35 mm petri dish to solidify with ~2 mm thickness. A 1 cm × 1 cm pad area was cut out, soaked in L-15 medium overnight at 4 °C for equilibration, and warmed to 37°C just before use. Cells were plated on 14 or 20 mm glass microwell uncoated dishes before imaging. A flat metaphase cell was chosen among 80 - 100% confluent cells for pre-perturbation imaging. After imaging of the metaphase cell before compression, the pad was deposited gently, centered on the cell. Note: it is important to do this step gently and with minimal moving of the dish so the position of the cell could stay intact. Using an oil hydraulic fine manipulator (InjectMan 4, micromanipulator with dynamic movement control, 100–240 V/50–60 Hz) and a coarse manipulator attached to the confocal microscope. A metal rod (which is a part of micromanipulator where the needle for microinjection is inserted) was centered on the cell and lowered (z-axis) until weak contact was made with the pad (rod diameter ≫ cell diameter). The rod was lowered slowly (over ~10 s) for several μm until the cell area expanded, and its position kept constant as the cell and spindle responses were imaged. HeLa PRC1-GFP cells were imaged every 30 seconds for 3 times which gave us 4 different times the cell was imaged at: before compression , 0.5 min after compression, 1 min after compression and 1.5 minute after compression. Cell health was monitored through the presence of the intact cell membrane and the ability of the cell to enter anaphase after perturbation. Rough estimate of the number of vertically oriented metaphase spindles in a 35 mm petri dish is around 1 spindle per 50-100 horizontally oriented metaphase spindles. From 31 spindles that were compressed in about 45 independent experiments, 23 spindles rotated during the first 30 seconds of compression and could not be used for further analysis. From 8 spindles that remained vertically oriented during compression, 2 spindles were not compressed enough which was determined by their length. Successful compression, where spindle length decreased

for 0.5 microns or more, was achieved on 6 spindles from 5 independent experiments, which were then used for the analysis.

Confocal microscopy

Live RPE1 and HeLa cells were imaged using Bruker Opterra Multipoint Scanning Confocal Microscope (Buca et al., 2017) (Bruker Nano Surfaces, Middleton, WI, USA). The system was mounted on a Nikon Ti-E inverted microscope equipped with a Nikon CFI Plan Apo VC ×100/1.4 numerical aperture oil objective (Nikon, Tokyo, Japan). During imaging, cells were maintained at 37°C in Okolab Cage Incubator (Okolab, Pozzuoli, NA, Italy). A 22 µm slit aperture was used for RPE1 and 60 µm pinhole for HeLa cells. The xy-pixel size was 83 nm. For excitation of GFP and mCherry fluorescence, a 488 and a 561 nm diode laser line was used, respectively. For SiR-dyes, a 640 nm diode laser line was used. The excitation light was separated from the emitted fluorescence by using Opterra Dichroic and Barrier Filter Set 405/488/561/640. Images were captured with an Evolve 512 Delta EMCCD Camera (Photometrics, Tucson, AZ, USA) with no binning performed. To cover the whole metaphase spindle, z-stacks were acquired at 30–60 focal planes separated by 0.5 µm with unidirectional xyz scan mode. The system was controlled with the Prairie View Imaging Software (Bruker Nano Surfaces, Middleton, WI, USA).

Image and data analysis

To calculate spindle twist, microscopy images of horizontal spindles were analyzed in Fiji Software (ImageJ, National Institutes of Health, Bethesda, MD, USA) (Schindelin et al., 2012). Only images with both spindle poles in the same plane before and during imaging of the z-stack were used in analysis to avoid unspecific spindle movements in the calculation of spindle twist. Horizontal spindles were transformed into vertical orientation using a code written in R programming language in RStudio (Novak et al., 2018). In transformed stack microtubule bundles and poles appear as blobs.

Visual assessment. In this method, the spindle is observed end-on and the rotation of microtubule bundles around the pole-to-pole axis is estimated visually. If the bundles rotate clockwise when moving along the spindle axis in the direction towards the observer, the twist is left-handed, and vice versa (Fig. S1A, left). The outcome of our visual assessment is a score of spindle twist, which describes whether the spindle has a strong left-handed, weak left-handed, strong right-handed, weak right-handed, or no visible twist. The advantage of this method is its trustworthiness because coarse classification of spindles into 5 groups is reliable, whereas the main disadvantage is that the results are semi-quantitative rather than quantitative.

Optical flow. In the optical flow method, the movement of the signal coming from microtubule bundles is estimated automatically by comparing the signal from one z-plane to the next (Fig. S1A, middle). This method yields a value for the average twist of all bundles in a spindle. It is the preferred choice for experiments on a large number of spindles because it is

automated. Disadvantages are that it provides only the average twist value rather than the twist of each bundle, and that the results are sensitive to unspecific signal in the images, individual bundles with atypical behavior, and imperfect alignment of the spindle axis with the z-axis.

First, parts of the images containing the blobs were selected for analysis using Rectangle tool in ImageJ. In all transformed stacks only images between spindle poles were used for analysis. Transformed spindle images contained a lot of noise that was removed by using the Mexican hat filter and a threshold. The Mexican hat filter, also called the LoG (Laplacian of Gaussian) filter, was used for detection of blobs (Jin and Feng, 2014; Lowe, 2004). After applying the Mexican hat filter, a threshold was applied to the image. It removes all the pixels with intensity lower than the given threshold. Microtubule bundles of transformed spindles were detected and traced automatically using optical flow for calculating the movement of pixels between two consecutive images. Farnebäck's two-frame motion estimation algorithm (dense optical flow algorithm) was used (Farnebäck, 2003). Only spindle poles were tracked manually using Multipoint tool in ImageJ. Helicities of mitotic spindles were calculated using algorithm called All pixels helicity algorithm. It calculates the total helicity as the average helicity of all pixels in the spindle. The code for tracing of bundles and helicity calculating was written in Python programming languange using PyCharm IDE. The external libraries used in image preprocessing, calculating helicity and visualisation are NumPy, scikit-image, Matplotib, PIL, OpenCV and SciPy. The code and instructions are available at https://gitlab.com/IBarisic/detecting-microtubules-helicity-in-microscopic-3d-mages/tree/master.

Bundle tracing. Bundles in images of spindles oriented vertically were traced manually using Multipoint tool in Fiji (Novak et al., 2018). We convert the imaging plane (z-plane) to its corresponding z-coordinate by multiplying with the distance between successive planes set during image acquisition (0.5 μm) and by a factor of 0.81 to correct for the refractive index mismatch (Novak et al., 2018). Next, to describe the shape of a microtubule bundle, we use the method described in (Ivec et al., 2021). We first fit a plane to the points representing the bundle, and then we fit a circle that lies in this plane to the same points. From these fits we calculate the curvature and twist of the bundle as follows: (i) The curvature is calculated as one over the radius, and (ii) the twist is calculated as the angle between the plane and the z-axis divided by the mean distance of these points from the z-axis. Contour length of the bundle was calculated as the length of the fitted circular arc plus the distance of bundle ends from the corresponding poles. The main advantage of this method is that it yields a value of twist for each individual bundle in the spindle, whereas the main disadvantage is that it requires manual tracing, which makes it impractical for high-throughput studies.

To measure spindle length and width, we used the Line tool in Fiji. Length was measured by drawing a line from pole to pole of the spindle. Width in HeLa cells expressing PRC1-GFP was measured by drawing a line across the equatorial plane of the spindle, with the line ending at the outer edges of a spindle. Width in RPE1 cells expressing CENP-A-GFP and centrin1-GFP was measured by drawing a line across the equatorial plane of the spindle, with the line ending at

the outer kinetochore pairs.

To quantify protein expression, the fluorescence intensity signal of the protein of interest was measured on the whole spindle region using ImageJ Polygon Selection tool on the sum-intensity projection of the whole z-stack. The mean background fluorescence intensity measured in the cytoplasm was subtracted from the mean value obtained on the spindle, and the resulting value was divided by the number of z-slices used in the sum projection.

Statistical analysis

Fiji was used to scale images and adjust brightness and contrast. Figures were assembled in Adobe Illustrator CS5 and CC (Adobe Systems, Mountain View, CA, USA). Graphs were plotted in MATLAB (MathWorks, Natick, MA, USA). For generation of univariate scatter plots, the open "UnivarScatter" Matlab extension was used (https://github.com/manulera/UnivarScatter). Data are given as mean ± s.e.m., unless otherwise stated. Significance of data was estimated by Student's t-test (two-tailed and two sample unequal-variance; except for the experiments with spindle compression, where a paired t-test was used to compare the values for the same spindles before and after compression). $p < 0.05$ was considered statistically significant. Values of all significant differences are given with degree of significance indicated (*$0.01 < p < 0.05$, **$0.001 < p < 0.01$, ***$p < 0.001$). Statistically significant differences between groups of data were determined by one-way ANOVA and Tukey's HSD post hoc test, $p < 0.05$ was considered statistically significant. The number of analyzed cells and microtubule bundles is given in the respective figure panel.

REFERENCES

Asbury, C.L. 2017. Anaphase A: Disassembling Microtubules Move Chromosomes toward Spindle Poles. *Biology (Basel)*. 6.

Bormuth, V., B. Nitzsche, F. Ruhnow, A. Mitra, M. Storch, B. Rammner, J. Howard, and S. Diez. 2012. The highly processive kinesin-8, Kip3, switches microtubule protofilaments with a bias toward the left. *Biophys J*. 103:L4-6.

Brunnbauer, M., R. Dombi, T.H. Ho, M. Schliwa, M. Rief, and Z. Okten. 2012. Torque generation of kinesin motors is governed by the stability of the neck domain. *Mol Cell*. 46:147-158.

Buda, R., K. Vukusic, and I.M. Tolic. 2017. Dissection and characterization of microtubule bundles in the mitotic spindle using femtosecond laser ablation. *Method Cell Biol*. 139:81-101.

Bugiel, M., E. Bohl, and E. Schaffer. 2015. The Kinesin-8 Kip3 switches protofilaments in a sideward random walk asymmetrically biased by force. *Biophys J*. 108:2019-2027.

Can, S., M.A. Dewitt, and A. Yildiz. 2014. Bidirectional helical motility of cytoplasmic dynein around microtubules. *Elife*. 3:e03205.

David, A.F., P. Roudot, W.R. Legant, E. Betzig, G. Danuser, and D.W. Gerlich. 2019. Augmin accumulation on long-lived microtubules drives amplification and kinetochore-directed growth. *J Cell Biol*. 218:2150-2168.

Dogterom, M., and B. Yurke. 1997. Measurement of the force-velocity relation for growing microtubules. *Science*. 278:856-860.

Dumont, S., and T.J. Mitchison. 2009. Force and length in the mitotic spindle. *Curr Biol*. 19:R749-761.

Farnebäck, G. 2003. Two-Frame Motion Estimation Based on Polynomial Expansion. Springer Berlin Heidelberg, Berlin, Heidelberg. 363-370.

Gittes, F., B. Mickey, J. Nettleton, and J. Howard. 1993. Flexural rigidity of microtubules and actin filaments measured from thermal fluctuations in shape. *J Cell Biol*. 120:923-934.

Goshima, G., M. Mayer, N. Zhang, N. Stuurman, and R.D. Vale. 2008. Augmin: a protein complex required for centrosome-independent microtubule generation within the spindle. *J Cell Biol*. 181:421-429.

Hewitt, L., A. Tighe, S. Santaguida, A.M. White, C.D. Jones, A. Musacchio, S. Green, and S.S. Taylor. 2010. Sustained Mps1 activity is required in mitosis to recruit O-Mad2 to the Mad1-C-Mad2 core complex. *J Cell Biol*. 190:25-34.

Howard, J. 2001. Mechanics of motor proteins and the cytoskeleton. Sinauer Associates, Sunderland, Mass. xvi, 367 p. pp.

Ivec, A., M. Trupinić, I.M. Tolić, and N. Pavin. 2021. Oblique circle method for measuring the curvature and twist of mitotic spindle microtubule bundles. *Biophys J,* in press. *https://doi.org/10.1016/j.bpj.2021.07.024.*

Jagric, M., P. Risteski, J. Martincic, A. Milas, and I.M. Tolic. 2021. Optogenetic control of PRC1 reveals its role in chromosome alignment on the spindle by overlap length-dependent forces. *Elife*. 10.

Jiang, W., G. Jimenez, N.J. Wells, T.J. Hope, G.M. Wahl, T. Hunter, and R. Fukunaga. 1998. PRC1: a human mitotic spindle-associated CDK substrate protein required for cytokinesis. *Mol Cell*. 2:877-885.

Jin, F., and D.Z. Feng. 2014. Image Registration Algorithm Using Mexican Hat Function-Based Operator and Grouped Feature Matching Strategy. *Plos One*. 9.

Kajtez, J., A. Solomatina, M. Novak, B. Polak, K. Vukusic, J. Rudiger, G. Cojoc, A. Milas, I. Sumanovac Sestak, P. Risteski, F. Tavano, A.H. Klemm, E. Roscioli, J. Welburn, D. Cimini, M. Gluncic, N. Pavin, and I.M. Tolic. 2016. Overlap microtubules link sister k-fibres and balance the forces on bi-oriented kinetochores. *Nat Commun*. 7:10298.

Kamasaki, T., E. O'Toole, S. Kita, M. Osumi, J. Usukura, J.R. McIntosh, and G. Goshima. 2013. Augmin-dependent microtubule nucleation at microtubule walls in the spindle. *J Cell Biol*. 202:25-33.

Liu, X., and M. Winey. 2012. The MPS1 family of protein kinases. *Annu Rev Biochem*. 81:561-585.

Lowe, D.G. 2004. Distinctive image features from scale-invariant keypoints. *Int J Comput Vision*. 60:91-110.

Maiato, H., A.M. Gomes, F. Sousa, and M. Barisic. 2017. Mechanisms of Chromosome Congression during Mitosis. *Biology (Basel)*. 6.

Manenica, M., V. Štimac, I. Koprivec, J. Simunic, and I.M. Tolic. 2020. Augmin regulates kinetochore tension and spatial arrangement of spindle microtubules by nucleating bridging fibers. *doi: https://doi.org/10.1101/2020.09.10.291740*.

Mann, B.J., and P. Wadsworth. 2018. Distribution of Eg5 and TPX2 in mitosis: Insight from CRISPR tagged cells. *Cytoskeleton (Hoboken)*. 75:508-521.

Maruyama, Y., M. Sugawa, S. Yamaguchi, T. Davies, T. Osaki, T. Kobayashi, M. Yamagishi, S. Takeuchi, M. Mishima, and J. Yajima. 2021. CYK4 relaxes the bias in the off-axis motion by MKLP1 kinesin-6. *Commun Biol*. 4:180.

McIntosh, J.R., M.I. Molodtsov, and F.I. Ataullakhanov. 2012. Biophysics of mitosis. *Q Rev Biophys*. 45:147-207.

Mitra, A., L. Meissner, R. Gandhimathi, R. Renger, F. Ruhnow, and S. Diez. 2020. Kinesin-14 motors drive a right-handed helical motion of antiparallel microtubules around each other. *Nat Commun*. 11:2565.

Mitra, A., F. Ruhnow, S. Girardo, and S. Diez. 2018. Directionally biased sidestepping of Kip3/kinesin-8 is regulated by ATP waiting time and motor-microtubule interaction strength. *Proc Natl Acad Sci U S A*. 115:E7950-E7959.

Neahring, L., N.H. Cho, and S. Dumont. 2021. Opposing motors provide mechanical and functional robustness in the human spindle. *https://doi.org/10.1101/2021.03.02.433652*.

Nicklas, R.B. 1983. Measurements of the force produced by the mitotic spindle in anaphase. *J Cell Biol*. 97:542-548.

Novak, M., B. Polak, J. Simunic, Z. Boban, B. Kuzmic, A.W. Thomae, I.M. Tolic, and N. Pavin. 2018. The mitotic spindle is chiral due to torques within microtubule bundles. *Nat Commun*. 9:3571.

Nurse, P. 2000. A long twentieth century of the cell cycle and beyond. *Cell*. 100:71-78.

Pavin, N., and I.M. Tolic. 2016. Self-Organization and Forces in the Mitotic Spindle. *Annu Rev Biophys*. 45:279-298.

Pavin, N., and I.M. Tolic. 2021. Mechanobiology of the Mitotic Spindle. *Dev Cell*. 56:192-201.

Petry, S., A.C. Groen, K. Ishihara, T.J. Mitchison, and R.D. Vale. 2013. Branching microtubule nucleation in Xenopus egg extracts mediated by augmin and TPX2. *Cell*. 152:768-777.

Polak, B., P. Risteski, S. Lesjak, and I.M. Tolic. 2017. PRC1-labeled microtubule bundles and kinetochore pairs show one-to-one association in metaphase. *EMBO Rep*. 18:217-230.

Prosser, S.L., and L. Pelletier. 2017. Mitotic spindle assembly in animal cells: a fine balancing act. *Nat Rev Mol Cell Biol*. 18:187-201.

Ramaiya, A., B. Roy, M. Bugiel, and E. Schaffer. 2017. Kinesin rotates unidirectionally and generates torque while walking on microtubules. *Proc Natl Acad Sci U S A*. 114:10894-10899.

Risteski, P., M. Jagric, N. Pavin, and I.M. Tolic. 2021. Biomechanics of chromosome alignment at the spindle midplane. *Curr Biol*. 31:R574-R585.

Rubinstein, B., K. Larripa, P. Sommi, and A. Mogilner. 2009. The elasticity of motor-microtubule bundles and shape of the mitotic spindle. *Phys Biol*. 6:016005.

Schindelin, J., I. Arganda-Carreras, E. Frise, V. Kaynig, M. Longair, T. Pietzsch, S. Preibisch, C. Rueden, S. Saalfeld, B. Schmid, J.Y. Tinevez, D.J. White, V. Hartenstein, K. Eliceiri, P. Tomancak, and A. Cardona. 2012. Fiji: an open-source platform for biological-image analysis. *Nat Methods*. 9:676-682.

Scholey, J.M., G. Civelekoglu-Scholey, and I. Brust-Mascher. 2016. Anaphase B. *Biology (Basel)*. 5.

Simunic, J., and I.M. Tolic. 2016. Mitotic Spindle Assembly: Building the Bridge between Sister K-Fibers. *Trends Biochem Sci*. 41:824-833.

Stumpff, J., G. von Dassow, M. Wagenbach, C. Asbury, and L. Wordeman. 2008. The kinesin-8 motor Kif18A suppresses kinetochore movements to control mitotic chromosome alignment. *Dev Cell*. 14:252-262.

Tolic-Norrelykke, I.M. 2008. Push-me-pull-you: how microtubules organize the cell interior. *Eur Biophys J*. 37:1271-1278.

Tolic, I.M. 2018. Mitotic spindle: kinetochore fibers hold on tight to interpolar bundles. *Eur Biophys J*. 47:191-203.

Tolic, I.M., M. Novak, and N. Pavin. 2019. Helical Twist and Rotational Forces in the Mitotic Spindle. *Biomolecules*. 9.

Uehara, R., R.S. Nozawa, A. Tomioka, S. Petry, R.D. Vale, C. Obuse, and G. Goshima. 2009. The augmin complex plays a critical role in spindle microtubule generation for mitotic progression and cytokinesis in human cells. *Proc Natl Acad Sci U S A*. 106:6998-7003.

Vale, R.D., and Y.Y. Toyoshima. 1988. Rotation and translocation of microtubules in vitro induced by dyneins from Tetrahymena cilia. *Cell*. 52:459-469.

Valentine, M.T., P.M. Fordyce, and S.M. Block. 2006. Eg5 steps it up! *Cell Div*. 1:31.

Velle, K.B., M. Trupinić, A. Ivec, A. Swafford, E. Nolton, L. Rice, I.M. Tolić, L.K. Fritz-Laylin, and P. Wadsworth. 2021. *Naegleria*'s mitotic spindles are built from unique tubulins and highlight core spindle features. *https://doi.org/10.1101/2021.02.23.432318*.

Vukusic, K., R. Buda, A. Bosilj, A. Milas, N. Pavin, and I.M. Tolic. 2017. Microtubule Sliding within the Bridging Fiber Pushes Kinetochore Fibers Apart to Segregate Chromosomes. *Dev Cell*. 43:11-23 e16.

Vukusic, K., R. Buda, and I.M. Tolic. 2019. Force-generating mechanisms of anaphase in human cells. *J Cell Sci*. 132.

Vukusic, K., I. Ponjavic, R. Buda, P. Risteski, and I.M. Tolic. 2021. Microtubule-sliding modules based on kinesins EG5 and PRC1-dependent KIF4A drive human spindle elongation. *Dev Cell*. 56:1253-1267 e1210.

Vukusic, K., and I.M. Tolic. 2021. Anaphase B: Long-standing models meet new concepts. *Semin Cell Dev Biol*.

Walczak, C.E., I. Vernos, T.J. Mitchison, E. Karsenti, and R. Heald. 1998. A model for the proposed roles of different microtubule-based motor proteins in establishing spindle bipolarity. *Curr Biol*. 8:903-913.

Walker, R.A., E.D. Salmon, and S.A. Endow. 1990. The Drosophila claret segregation protein is a minus-end directed motor molecule. *Nature*. 347:780-782.

Yajima, J., and R.A. Cross. 2005. A torque component in the kinesin-1 power stroke. *Nat Chem Biol*. 1:338-341.

Yajima, J., K. Mizutani, and T. Nishizaka. 2008. A torque component present in mitotic kinesin Eg5 revealed by three-dimensional tracking. *Nat Struct Mol Biol*. 15:1119-1121.

ACKNOWLEDGEMENTS

We thank Ina Poser, Tony Hyman and Alexey Khodjakov for cell lines; Jason Stumpff and Casper C. Hoogenraad for plasmids; Juraj Simunić, Jurica Matković, Valentina Štimac, Isabella Koprivec, Lucija Bujanić and Iva Buljan for their contribution in experimental work; Martina Manenica for the help with the MATLAB codes, and Ivana Šarić for the drawings. We thank Nenad Pavin, Maja Novak and all members of Tolić and Pavin groups for helpful discussions. This work was funded by the European Research Council (ERC Consolidator Grant, GA Number 647077), the Croatian Science Foundation (HRZZ project IP-2019-04-5967), and the QuantiXLie Center of Excellence, a project co-financed by the Croatian Government and European Union through the European Regional Development Fund—the Competitiveness and Cohesion Operational Programme (Grant KK.01.1.1.01.0004). We also acknowledge new support by the ERC (Synergy Grant, GA Number 855158). The work of doctoral students M.T. and A.I. have been supported in part by the "Young researchers' career development project – training of doctoral students" of the Croatian Science Foundation.

AUTHOR CONTRIBUTIONS

M.T. performed experiments on RPE1 cells, B.K. and M.T. performed experiments on HeLa cells, except compression experiments, which were done by I.P. M.T., B.K. and I.P. analyzed the experimental data. I.B. and S.Š. developed the optical flow method for twist measurement. A.I. measured the twist from bundle traces. M.T. and I.M.T. wrote the manuscript, with input from I.P., B.K., and other authors. M.T. assembled the figures. I.M.T. conceived the project and supervised the experiments.

SUPPLEMENTARY INFORMATION

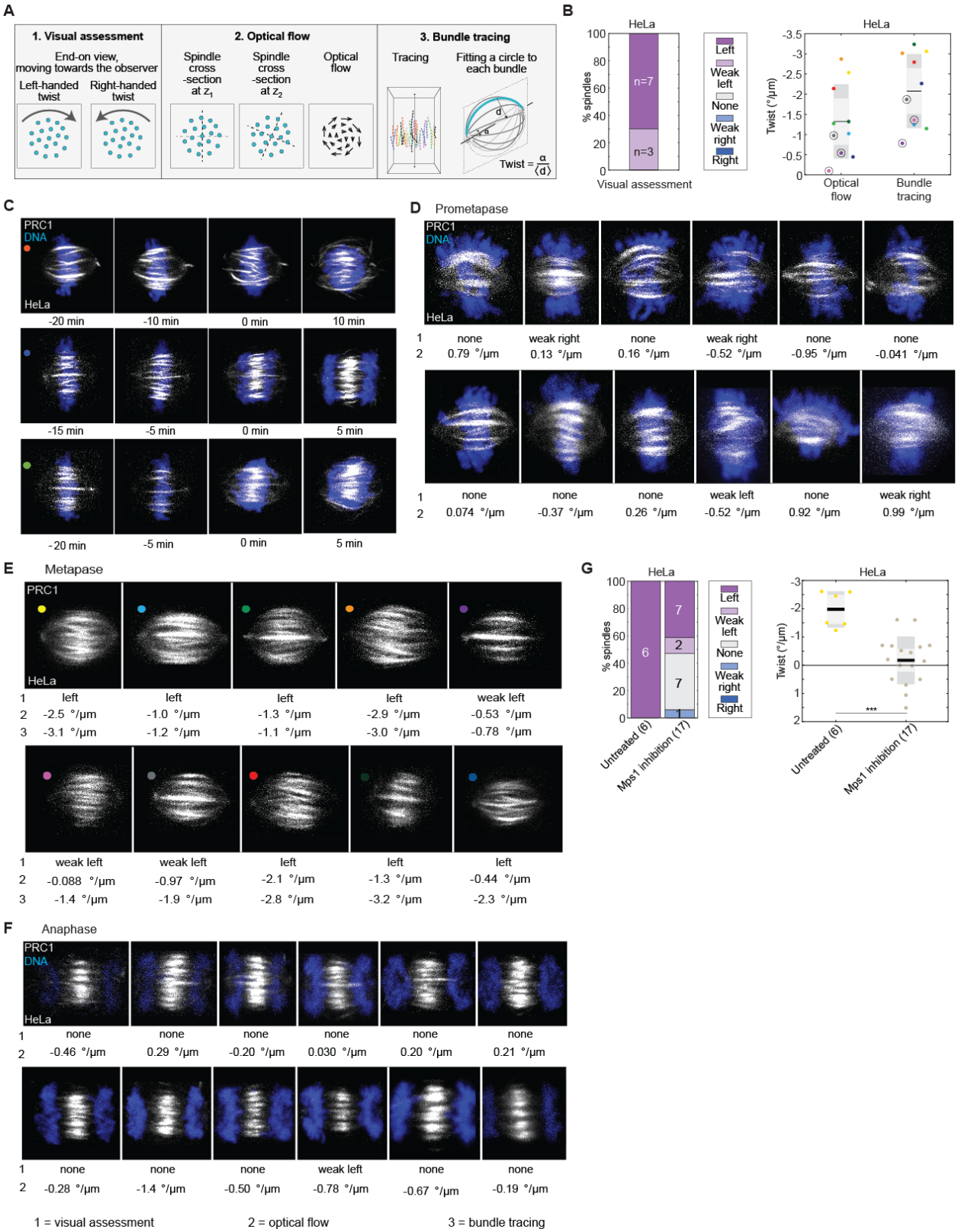

Figure S1. Methods for calculating twist and progression of twist during mitosis in HeLa cells.

(A) Schemes of three methods used to measure spindle twist: visual assessment (1), optical flow (2) and bundle tracing (3).

(B) Comparison of the twist for 10 spindles calculated with three different methods. On the left, visual assessment graph represents percentages of spindles showing left, right, weak left, weak right or no twist as described in the legend. On the right, graph shows twist calculated with optical flow and bundle tracing methods; each color represents one cell; circled and un-circled data correspond with the 'weak left' and 'left' data from the visual assessment graph, respectively. The black line shows the mean; the light and dark grey areas mark 95% confidence interval on the mean and standard deviation, respectively. Same cells were used to calculate the data for both methods. Experiments were performed on the HeLa-Kyoto BAC cells stably expressing PRC1-GFP (n=10; raw data taken and re-calculated from (Novak et al., 2018)).

(C) Microscope images of HeLa cells' spindles in time. Each colored dot represents one spindle's progression through mitosis in time, and each color matches the color of the spindle's data in the graph in Fig. 1C. Three individual examples are shown. Microtubule bundles are shown in grey (PRC1-GFP) and DNA in blue (SiR-DNA dye). Images are shown in maximum z-projections. Experiments were performed on the HeLa-Kyoto BAC cells stably expressing PRC1-GFP.

(D-F) Microscope images of individual **s**pindles of HeLa cells in different phases of mitosis. Examples of spindles in prometaphase (D), metaphase (E) and anaphase (F) are shown with their twist values. Twist was determined with the visual assessment method and the optical flow, marked 1 and 2, respectively. For metaphase spindles twist was also calculated using bundle tracing method, marked 3. Data from these cells was used in the graphs in Fig. 1D. Data from metaphase cells was also used in Fig. S1B. Microtubule bundles are shown in grey (PRC1-GFP) and DNA in blue (SiR-DNA dye). Images are shown in maximum z-projections. Experiments were performed on the HeLa-Kyoto BAC cells stably expressing PRC1-GFP.

(G) Graphs showing twist values after the inhibition of Mps1 in HeLa cells. On the left, visual assessment graph represents percentages of spindles showing left, right, weak left, weak right or no twist as described in the legend. On the right, graph shows twist calculated with the optical flow method. The black line shows the mean; the light and dark grey areas mark 95% confidence interval on the mean and standard deviation, respectively. ***$p<0.001$ (Student's t-test). Experiments were performed on the HeLa-Kyoto BAC cells stably expressing PRC1-GFP.

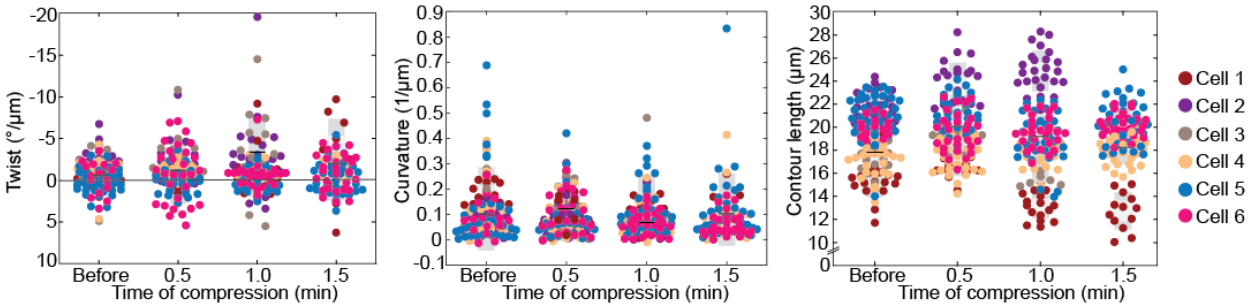

Figure S2. Twist, curvature and contour length of microtubule bundles in spindles compressed by an external force.

On the left, graph show the change of the twist before and up to 1.5 min after the compression. In the middle, graph shows the change of the curvature before and up to 1.5 min after the compression. On the right, graph shows the change of length of the bundle contours before and up to 1.5 min after the compression. Each color represents one cell, as described in the legend; dots represent bundles; the black line shows the mean; the light and dark grey areas mark 95% confidence interval on the mean and standard deviation, respectively. Experiments were performed on the HeLa-Kyoto BAC cells stably expressing PRC1-GFP.

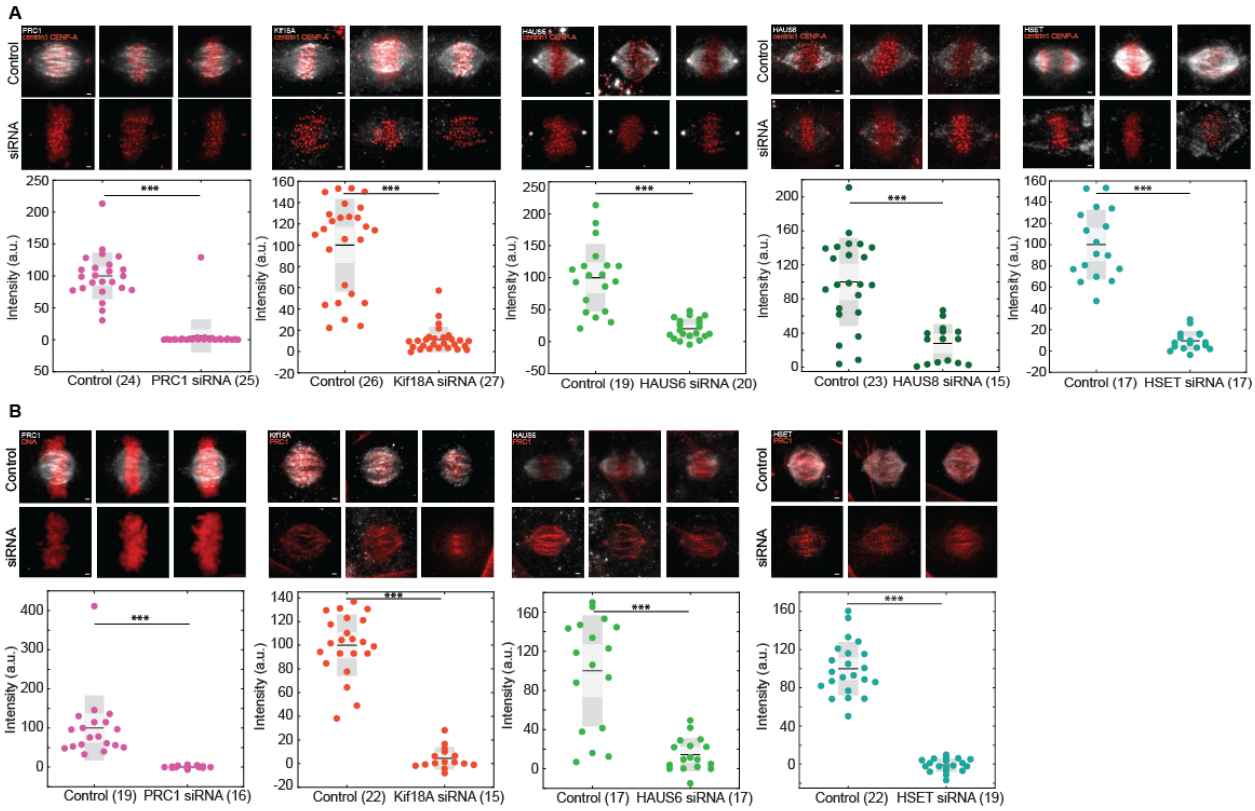

Figure S3. Immunofluorescence images of spindles in RPE1 and HeLa cells after protein perturbations.

(A) Immunofluorescence of RPE1 cells' spindles after perturbation of spindle-associated proteins. Examples of three spindles for every perturbation of spindle-associated proteins and their controls: Kif18A depletion, PRC1 depletion, HAUS6, HAUS8 depletion and HSET depletion, in that order. Microtubule bundles are shown in grey (proteins of interest) and kinetochores/centrosomes in red. Images are shown in maximum z-projections. Graphs show intensities of protein of interest in control cells and cells treated with siRNA. ***p<0.001 (Student's t-test). Experiments were performed on the hTERT-RPE1 cells, permanently transfected and stabilized using CENP-A-GFP and centrin1-GFP.

(B) Immunofluorescence of HeLa cells' spindles after perturbation of spindle-associated proteins. Examples of three spindles for every perturbation of spindle-associated proteins and their controls: Kif18A depletion, PRC1 depletion, HAUS6 and HSET depletion, in that order. Microtubule bundles are shown in grey (proteins of interest) and DNA (dyed with DAPI in non-transfected HeLa) or PRC1 (in HeLa-Kyoto BAC cells stably expressing PRC1-GFP) in red. Images are shown in maximum z-projections. Graphs show intensities of protein of interest in control cells and cells treated with siRNA. ***p<0.001 (Student's t-test). Experiments were performed on the non-transfected HeLa cell line (for the depletion of PRC1 and its control) and HeLa-Kyoto BAC cells stably expressing PRC1-GFP (for the rest of the treatments).

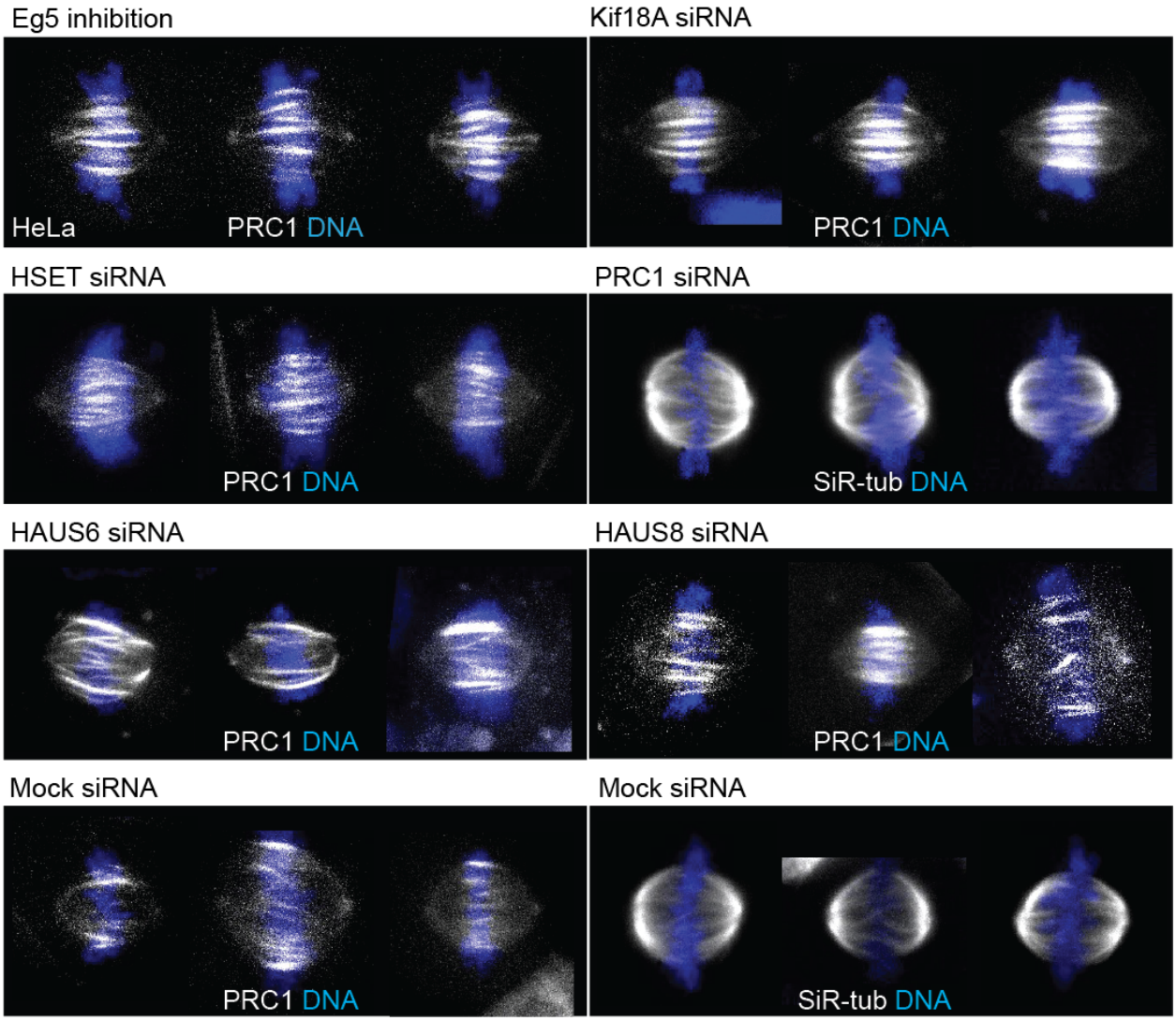

Figure S4. Spindles of HeLa cells after perturbation of spindle-associated proteins.
Examples of three spindles for every perturbation of spindle-associated proteins: Eg5 inhibition, Kif18A depletion, HSET depletion, PRC1 depletion, HAUS6 and HAUS8 depletion and mock controls. Data was used in the graphs in Figs. 3B and 4B. Microtubule bundles are shown in grey (SiR-tubulin in non-transfected HeLa and PRC1-GFP in HeLa-Kyoto BAC cell line) and DNA in blue (SiR-DNA dye). Images are shown in maximum z-projections. Experiments were performed on the non-tranfected HeLa cell line and HeLa-Kyoto BAC cells stably expressing PRC1-GFP.

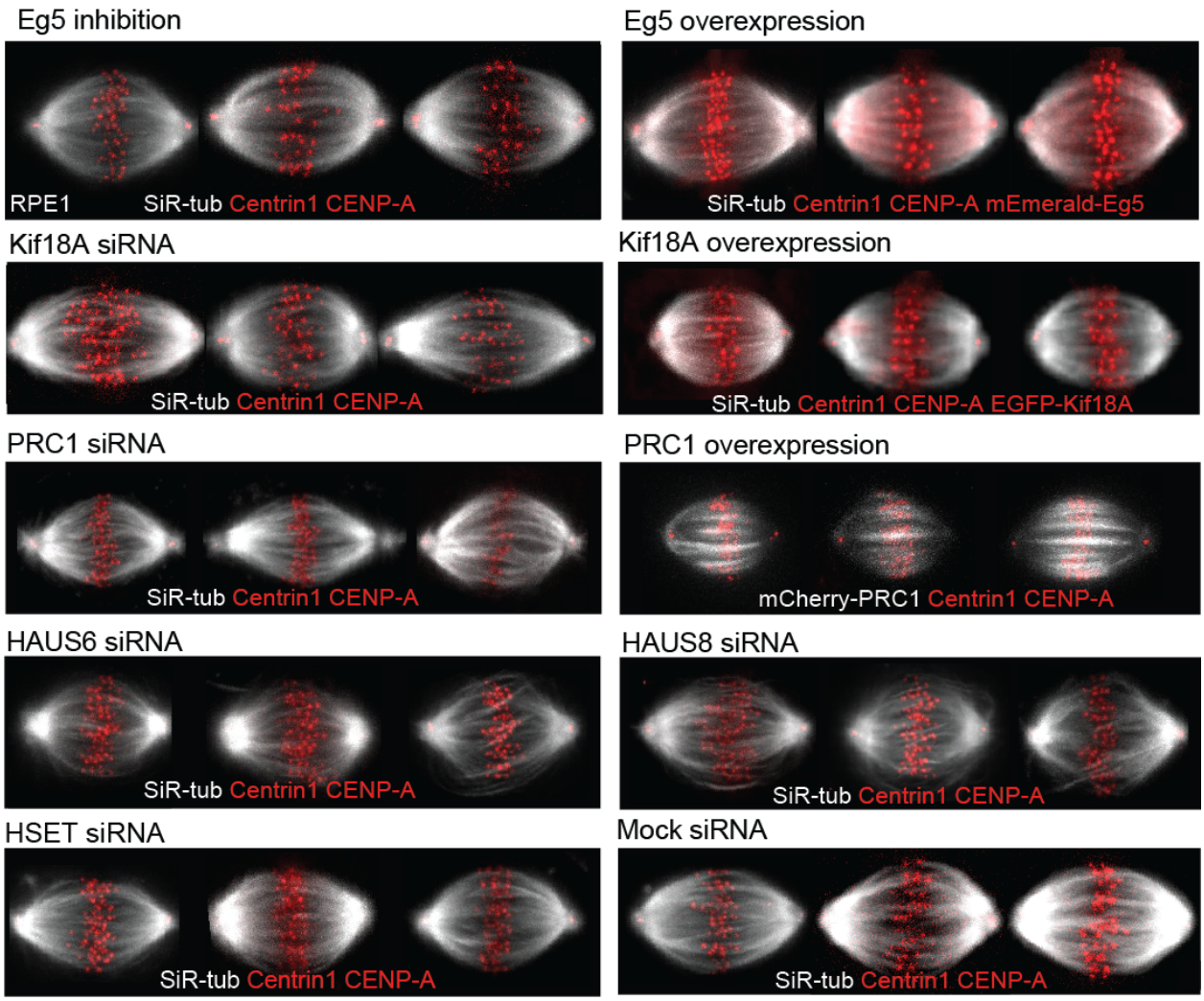

Figure S5. Spindles of RPE1 cells after perturbation of spindle-associated proteins.
Examples of three spindles for every perturbation of spindle-associated proteins: Eg5 inhibition, Eg5 overexpression, Kif18A depletion, Kif18A overexpression, PRC1 depletion, PRC1 overexpression, HAUS6 and HAUS8 depletion, HSET depletion and mock control. Data was used in the graphs in Fig. 3C and 4C. Microtubule bundles are shown in grey (SiR-tubulin and, for PRC1 overexpression, mCherry-PRC1) and kinetochores/centrosomes, Eg5 and KiF18A in red. Images are shown in maximum z-projections. Experiments were performed on the hTERT-RPE1 cells, permanently transfected and stabilized using CENP-A-GFP and centrin1-GFP.

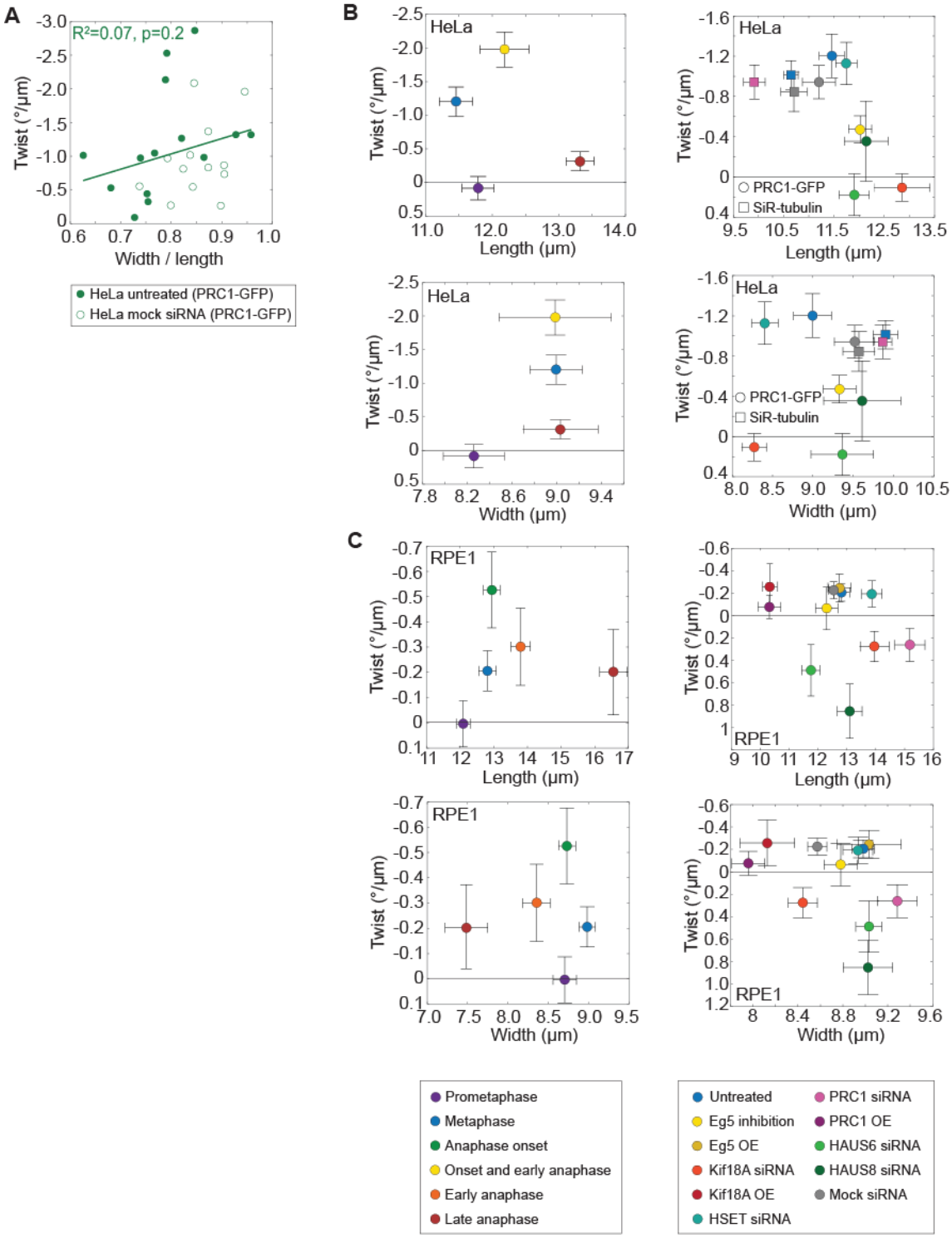

Figure S6. Correlation between spindle length or width and spindle twist in different phases of mitosis and during different protein perturbations in HeLa and RPE1 cells.

(A) Round spindles have stronger twist than elongated spindles. Graph shows the correlation between width/length ratio and twist in HeLa cells. Filled circles represent untreated cells while empty circles

represent mock siRNA controls. Lines show linear fit (untreated cells together with mock siRNA controls); equation y=-2.28x+0.79; goodness of fit shown in the graph. Same data was used in Figs. 1D, 3B and 4B. Experiments were performed on the HeLa-Kyoto BAC cells stably expressing PRC1-GFP.

(B) Graphs showing how the spindle twist and length (top) or width (bottom) in HeLa cells vary depending on the different phases of mitosis (left) or perturbations of spindle-associated proteins (right). Each color represents different phase of mitosis or protein perturbation, as described in the legend at the bottom; error bars represent SEM. Same data was used in graphs in Fig. 1D, 3B and 4B. Experiments were performed on the HeLa-Kyoto BAC cells stably expressing PRC1-GFP (dots) and non-tranfected HeLa cell line for the depletion of PRC1 and its controls (rectangles).

(C) Graphs showing how the spindle twist and length (top) or width (bottom) in RPE1 cells vary depending on the different phases of mitosis (left) or perturbations of spindle-associated proteins (right). Each color represents different phase of mitosis or protein perturbation, as described in the legend at the bottom; error bars represent SEM. Same data was used in graphs in Fig. 1E, 3C and 4C. Experiments were performed on the hTERT-RPE1 cells, permanently transfected and stabilized using CENP-A-GFP and centrin1-GFP.

MOVIE CAPTIONS

Movie S1: Left-handed twist of the mitotic spindle in human cell. On the left, scheme of end-on point of view of the spindle; plane shows movement through z-planes. On the right, end-on view of fixed HeLa cell expressing PRC1-GFP (PRC1-GFP signal not shown); arrowheads point at the microtubule bundles that twist in a clockwise direction (indication of left-handed twist). Microtubule bundles are shown in grey; anti-α-tubulin in HeLa cell. Image of the spindle is shown in Fig. 1A.

Movie S2: Twist of prometaphase spindles. On the left, side-view (top) and end-on view (bottom) of prometaphase spindle in HeLa cell expressing PRC1-GFP; microtubule bundles are shown in grey (PRC1-GFP) and DNA in blue (SiR-DNA dye). On the right, side-view (top) and end-on view (bottom) of prometaphase spindle in RPE1 cells expressing CENP-A-GFP and centrin1-GFP; microtubule bundles are shown in grey (SiR-tubulin dye) and kinetochores/centrosomes (CENP-A-GFP/centrin-1-GFP) in red. Movies of spindles shown from the side view are played once while movies of spindles shown from the end-on view are repeated three times. Scale bar, 1 μm. Images of spindles are shown in Fig. 1B.

Movie S3: Twist of metaphase spindles. On the left, side-view (top) and end-on view (bottom) of metaphase spindle in HeLa cell expressing PRC1-GFP; microtubule bundles are shown in grey (PRC1-GFP) and DNA in blue (SiR-DNA dye). On the right, side-view (top) and end-on view (bottom) of metaphase spindle in RPE1 cells expressing CENP-A-GFP and centrin1-GFP; microtubule bundles are shown in grey (SiR-tubulin dye) and kinetochores/centrosomes (CENP-A-GFP/centrin-1-GFP) in red. Movies of spindles shown from the side view are played once while movies of spindles shown from the end-on view are repeated three times. Scale bar, 1 μm. Images of spindles are shown in Fig. 1B.

Movie S4: Twist of spindles at the beginning of anaphase. On the left, side-view (top) and end-on view (bottom) of the spindle at the beginning of anaphase in HeLa cell expressing PRC1-GFP; microtubule bundles are shown in grey (PRC1-GFP) and DNA in blue (SiR-DNA dye). On the right, side-view (top) and end-on view (bottom) of the spindle at the beginning of anaphase in RPE1 cells expressing CENP-A-GFP and centrin1-GFP; microtubule bundles are shown in grey (SiR-tubulin dye) and kinetochores/centrosomes (CENP-A-GFP/centrin-1-GFP) in red. Movies of spindles shown from the side view are played once while movies of spindles shown from the end-on view are repeated three times. Scale bar, 1 μm. Images of spindles are shown in Fig. 1B.

Movie S5: Twist of early anaphase spindles. On the left, side-view (top) and end-on view (bottom) of early anaphase spindle in HeLa cell expressing PRC1-GFP; microtubule bundles are shown in grey (PRC1-GFP) and DNA in blue (SiR-DNA dye). On the right, side-view (top) and end-on view (bottom) of early anaphase spindle in RPE1 cells expressing CENP-A-GFP and centrin1-GFP; microtubule bundles are shown in grey (SiR-tubulin dye) and kinetochores/centrosomes (CENP-A-GFP/centrin-1-GFP) in red. Movies of spindles shown from the side view are played once while movies of spindles shown from the end-on view are repeated three times. Scale bar, 1 μm. Images of spindles are shown in Fig. 1B.

Movie S6: Twist of late anaphase spindles. On the left, side-view (top) and end-on view (bottom) of late anaphase spindle in HeLa cell expressing PRC1-GFP; microtubule bundles are shown in grey (PRC1-GFP) and DNA in blue (SiR-DNA dye). On the right, side-view (top) and end-on view (bottom) of late anaphase spindle in RPE1 cells expressing CENP-A-GFP and centrin1-GFP; microtubule bundles are shown in grey (SiR-tubulin dye) and kinetochores/centrosomes (CENP-A-GFP/centrin-1-GFP) in red. Movies of spindles shown from the side view are played once while movies of spindles shown from the end-on view are repeated three times. Scale bar, 1 μm. Images of spindles are shown in Fig. 1B.

Movie S7: Twist before and after spindle compression. On the left, end-on view of the spindle in HeLa cell expressing PRC1-GFP before compression. On the right, end-on view of the spindle in HeLa cell expressing PRC1-GFP after 1 min of compression. Microtubule bundles are shown in grey (PRC1-GFP). Movies are played three times consecutively. Scale bar, 1 μm. Traces representing microtubule bundles are shown in Fig. 2B.

Movie S8: Twist of spindles in cells with depleted Kif18A protein. On the left, side-view (top) and end-on view (bottom) of the spindle in HeLa cell, expressing PRC1-GFP, after the depletion of Kif18A protein; microtubule bundles are shown in grey (PRC1-GFP) and DNA in blue (SiR-DNA dye). On the right, side-view (top) and end-on view (bottom) of the spindle in RPE1 cells, expressing CENP-A-GFP and centrin1-GFP, after the depletion of Kif18A protein; microtubule bundles are shown in grey (SiR-tubulin dye) and kinetochores/centrosomes (CENP-A-GFP/centrin-1-GFP) in red. Movies of spindles shown from the side view are played once while movies of spindles shown from the end-on view are repeated three times. Scale bar, 1 μm. Images of spindles are shown in Fig. 3A.

Movie S9: Twist of spindles in cells with perturbed PRC1 protein. On the left, side-view (top) and end-on view (bottom) of the spindle in non-tranfected HeLa cell after the depletion of PRC1 protein; microtubule bundles are shown in grey (SiR-tubulin dye) and DNA in blue (SiR-DNA dye). In the middle, side-view (top) and end-on view (bottom) of the spindle in RPE1 cells, expressing CENP-A-GFP and centrin1-GFP, after the depletion of PRC1 protein; microtubule bundles are shown in grey (SiR-tubulin dye) and kinetochores/centrosomes (CENP-A-GFP/centrin-1-GFP) in red. On the right, side-view (top) and end-on view (bottom) of the spindle in RPE1 cells, expressing CENP-A-GFP and centrin1-GFP, after the overexpression of PRC1 protein; microtubule bundles are shown in grey (PRC1-mCherry) and kinetochores/centrosomes (CENP-A-GFP/centrin-1-GFP) in red. Movies of spindles shown from the side view are played once while movies of spindles shown from the end-on view are repeated three times. Scale bar, 1 μm. Images of spindles are shown in Fig. 4A.

Movie S10: Twist of spindles in cells with depleted HAUS8 protein. On the left, side-view (top) and end-on view (bottom) of the spindle with average twist value in HeLa cell, expressing PRC1-GFP, after the depletion of HAUS8 protein; microtubule bundles are shown in grey (PRC1-GFP) and DNA in blue (SiR-DNA dye). In the middle, side-view (top) and end-on view (bottom) of the spindle with high right-handed twist in HeLa cell, expressing PRC1-GFP, after the depletion of HAUS8 protein; microtubule bundles are shown in grey (PRC1-GFP) and DNA in blue (SiR-DNA dye). On the right, side-view (top) and end-on view (bottom) of the spindle in RPE1 cells, expressing CENP-A-GFP and centrin1-GFP, after the

depletion of HAUS8 protein; microtubule bundles are shown in grey (SiR-tubulin dye) and kinetochores/centrosomes (CENP-A-GFP/centrin-1-GFP) in red. Movies of spindles shown from the side view are played once while movies of spindles shown from the end-on view are repeated three times. Scale bar, 1 μm. Images of spindles are shown in Fig. 4A (except the spindle in HeLa cell with high right-handed twist).